Ricerca di Sistema elettrico

Sviluppo di un Modello di Combustione Generalizzato per la Large Eddy Simulation di Fiamme Premiscelate

E. Giacomazzi, D. Cecere, F.R. Picchia, N. Arcidiacono

SVILUPPO DI UN MODELLO DI COMBUSTIONE GENERALIZZATO PER LARGE EDDY SIMULATION

IN FIAMME PREMISCELATE

E. Giacomazzi, D. Cecere, F.R. Picchia, N. Arcidiacono (ENEA)

Settembre 2013

Indice

Sommario

E' stato sviluppato un nuovo modello di sottogriglia per Large Eddy Simulation per trattare l'interazione turbolenza / combustione in fiamme premiscelate. Questo modello ha l'ambizione di cogliere a livello locale (nello spazio) i regimi di combustione messi in evidenza dal classico diagramma di combustione premiscelata che riporta, in ascissa, il rapporto tra la scala integrale della turbolenza e lo spessore del fronte di fiamma, ed in ordinata, il rapporto tra la fluttuazione rms di velocità e la velocità di propagazione laminare del fronte stesso. L'obiettivo del modello è quello di stimare la frazione di volume reagente all'interno di ogni singola cella di calcolo. L'espressione finale di questa frazione dipende dal rapporto tra la velocità di propagazione turbolenta del fronte di fiamma e quella laminare, e dallo spessore del fronte di fiamma. Queste due fondamentali grandezze sono modellate diversamente in funzione del regime di combustione in cui la cella reagente viene a trovarsi. Il modello proposto definisce questi regimi di combustione sulla base di tre numeri caratteristici locali: il numero di Prandtl, quello di Reynolds e quello di Damkoheler. Sono anche considerati gli effetti di diffusione preferenziale delle specie combustibili più leggere, come l'idrogeno, sulla propagazione del fronte nelle regioni del flusso caratterizzate da bassi livelli di stiramento fluidodinamico. Oltre a considerare l'effetto positivo delle diverse scale turbolente sulla combustione, dovuto all'aumentato mescolamento ed eventuale inspessimento del fronte, il modello considera anche gli effetti negativi in termini di estinzione localizzata, dovuta allo stiramento del fronte di fiamma da parte dei vortici di piccola scala. Va osservato che il modello di estinzione adottato è stato ripreso da letteratura, dopo attenta valutazione dei modelli attualmente esistenti. Al momento della proposta del presente progetto, si pensava di validare il nuovo modello mediante il caso test di combustione premiscelata aria/syngas del PSI di Zurigo. In realtà i dati sperimentali relativi a tale caso sono insufficienti per una valutazione ed una validazione corretta del nuovo modello. Di conseguenza, è stato deciso di adottare inizialmente altri due casi test formalmente simili, ma aventi diversi numeri di Reynolds e quindi diversi livelli di turbolenza: una fiamma premiscelata metano / aria relativa ad un bruciatore con tre iniettori a sezione rettangolare affiancati. La miscela fresca reagente esce dall'iniettore centrale, mentre dai due restanti iniettori esce a velocità ridotta una miscela costituita dai gas prodotti dalla combustione della miscela centrale. Tali casi test sono più ricchi di dati con cui confrontarsi. Per la validazione occorrono una serie di simulazioni a diversi livelli di risoluzione spaziale. Le simulazioni sono ancora in corso e quindi la fase di validazione non è ancora conclusa. A valle di questa fase, si simulerà anche il combustore del PSI per focalizzare l'attenzione sugli effetti dovuti alla presenza dell'idrogeno.

1 Introduction

1.1 Combustion Regimes and the Klimov-Williams Diagram

A synthetic way to look at turbulence / combustion interaction consists in mapping what are possible combustion regimes. In fact, due to the complexity of multi-scale interaction between turbulence and chemistry, several combustion regimes may occur. Regime determination, i.e., the identification of the spatial structure and morphology of the reacting flow, is important for combustion modelling. Combustion regimes have been theoretically investigated for many years [1, 2, 3, 4, 5, 6, 7, 8] by simply assuming the turbulence integral length scale, L, the associated turbulent velocity fluctuation, u'_{rms}, the laminar flame speed, S_L, and the flame front thickness, δ_F, all defined or measured in some way, as the main quantities characterizing the turbulence - chemistry interaction. Such analysis is strictly valid only for premixed flames, because only for these flames it is possible to define the laminar flame speed S_L and the thickness of flame front δ_F.

A well established model of premixed turbulent combustion is in terms of laminar flamelets. The ``laminar flamelet'' concept is based on two assumptions. The first concerns with the topology of the flame; in particular, the reacting flow is viewed as a two-fluid flow (fresh and burnt gases) separated by an interface of finite thickness δ_F that is the flame (the limit $\delta_F \to 0$ leads to the ``infinitely-fast chemistry'' assumption). The second is about the flame structure: in particular, it is assumed that the flame front behaves locally just like a macroscopic laminar flame. If this flame is assumed planar and steady, the local burning rate is equal to the burning rate of steady planar laminar flames, whose characteristics may be predicted and then stored in flamelet libraries for modelling purposes. When only the first assumption is made, the regime is called ``extended flamelet'', i.e., the structure of the interface may not be necessarily assumed to be laminar. In general, a premixed turbulent flame can be thought to be in an ``extended flamelet'' regime when there is at least one flame front between fresh and burnt gases [9]. Thus, quenching determines the limit between ``flamelet'' or ``no flamelets'' (when quenching takes place) regime.

Analysis of combustion regimes is often based on intuitive, order-of-magnitude arguments in which, however, the physics of flame quenching plays a main role. Local flame quenching occurs when the burning rate inside the flame front becomes so low to slow down or completely suppress the combustion process. This may occur, for example, when a vortex of size $l > \delta_F$ distorts and stretches a flame ``front'', increasing its ``surface'' $\mathcal{A}$ and therefore the heat losses, thus producing extinction. Typically, combustion regimes are mapped in two dimensional diagrams showing regions where the flow structure will feature flamelets, pockets or distributed reaction zones. Just as typically, these diagrams do not include the effect of important flame physics such as heat losses, flame curvature, viscous dissipation and transient dynamics, all affecting quenching. Furthermore, the effect of the Lewis number on quenching produced by stretching is not considered [10, p. 56-59]. In literature there are several numerical simulations [11, 12] and experimental studies [13, 14, 15] on the effect of aerodynamic stretch on a laminar flame front (often a stagnation-point laminar flame, as shown in Fig. 1.1). These studies predict stretch factors, ζ, where

$$\zeta = (1/\mathcal{A}) \; d\mathcal{A}/dt \,, \qquad (1.1)$$

that produce extinction (and therefore are called critical stretch factors), showing that quenching is favoured by $Le > 1$ and by flame non-adiabaticity. A qualitative summary of these results is reported in Fig. 1.1. Understanding how stretch may quench a flame is important in modelling flame - vortex interaction, especially with a so-called flame surface model approach [16].
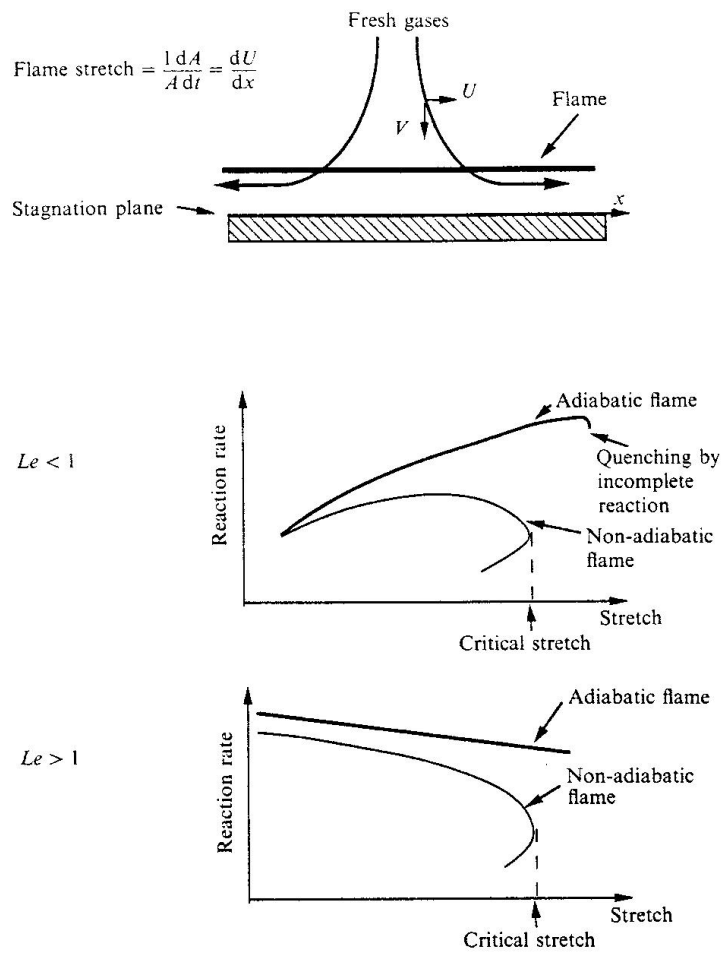
Figura 1.1: Effect of stretching on stagnation-point laminar flames [17].

A nondimensional parameter related to the effect of stretching on flame front is the Karlovitz number, defined as the ratio between the chemical time and the stretching time, and defined as

$$Ka_t = \frac{\tau_{ch}}{\tau_{st}} = \frac{\delta_F/S_L}{\left(\frac{1}{\mathcal{A}}\frac{d\mathcal{A}}{dt}\right)^{-1}} \ . \tag{1.2}$$

It is very useful to correlate data (e.g., on extinction) and is also intuitive: when $Ka_t > 1$ quenching may indeed occur and the reaction zone will be distributed: this is the so called Karlovitz criterion [18], today commonly referred to as Klimov-Williams criterion.

It is observed that the τ_{ch} used in Eqn. (1.2) is an overall chemical time. It is the local time required by reactants to be converted into hot products within the flame front thickness, or equivalently, it is the time associated to heat release at the scale $\sim \delta_F$. In real flames there is indeed a spectrum of chemical times, depending on the local state of the flow in terms of pressure, temperature and composition. This spectrum of chemical times is necessarily reduced just to one chemical time if S_L and δ_F are assumed constant; in fact, they are functions of local pressure, temperature and composition. Furthermore, the identity $\tau_{ch} \sim \delta_F/S_L$ neglects the effect of conductivity (or diffusivity more generally) on local laminar flame speed.

Because of the difficulty in calculating ζ as per its definition (1.1), in most works on turbulent flames, stretch is estimated from the rms velocity fluctuation and the Taylor microscale, i.e.,

$$\tau_{st} = \lambda_T/u'_{rms} \ . \tag{1.3}$$

Since the Taylor microscale is defined as

$$\lambda_T = L/Re_{L_t}^{1/2} \ , \tag{1.4}$$

L being the integral macroscale and Re_{L_t} the turbulent Reynolds number, defined as

$$Re_{L_t} = u'_{rms}L/\nu \ , \tag{1.5}$$

and remembering that from the simple Mallard - Le Chatelier laminar theory [19, p. 125-132]

$$S_L\delta_F/\nu = 1 \tag{1.6}$$

and also that, from Kolmogorov's theory [20], at the dissipative scale η

$$u_\eta\eta/\nu = 1 \ , \tag{1.7}$$

η being the Kolmogorov dissipative scale, i.e.,

$$\eta = L/Re_{L_t}^{3/4} \tag{1.8}$$

and u_η its characteristic velocity,

$$u_\eta = u'_{rms}/Re_{L_t}^{1/4} \ , \tag{1.9}$$

the Karlovitz number defined as in Eqn. (1.2) can be finally written as

$$Ka_t = \left(\frac{\delta_F}{\eta}\right)^2 \ . \tag{1.10}$$

This result can alternatively be found by assuming that the characteristic stretching time be the characteristic time τ_η of the Kolmogorov scale (that is, the inverse of the strain rate at the η scale), i.e.,

$$\tau_{st} = \lambda_T/u'_{rms} \equiv \eta/u_\eta \ . \tag{1.11}$$

By defining the Karlovitz number as in Eqn. (1.10) it is assumed that the η scales are the most important or effective in stretching a flame. Therefore, Ka_t, based on Eqn. (1.10), will be referred to as Ka_{η_t}. In a $log\left(u'_{rms}/S_L\right)$ vs $log\left(L/\delta_F\right)$ plane, the Ka_{η_t} curve is $log\left(u'_{rms}/S_L\right) = (1/3)\ log\left(L/\delta_F\right) + (2/3)\ logKa_{\eta_t}$.
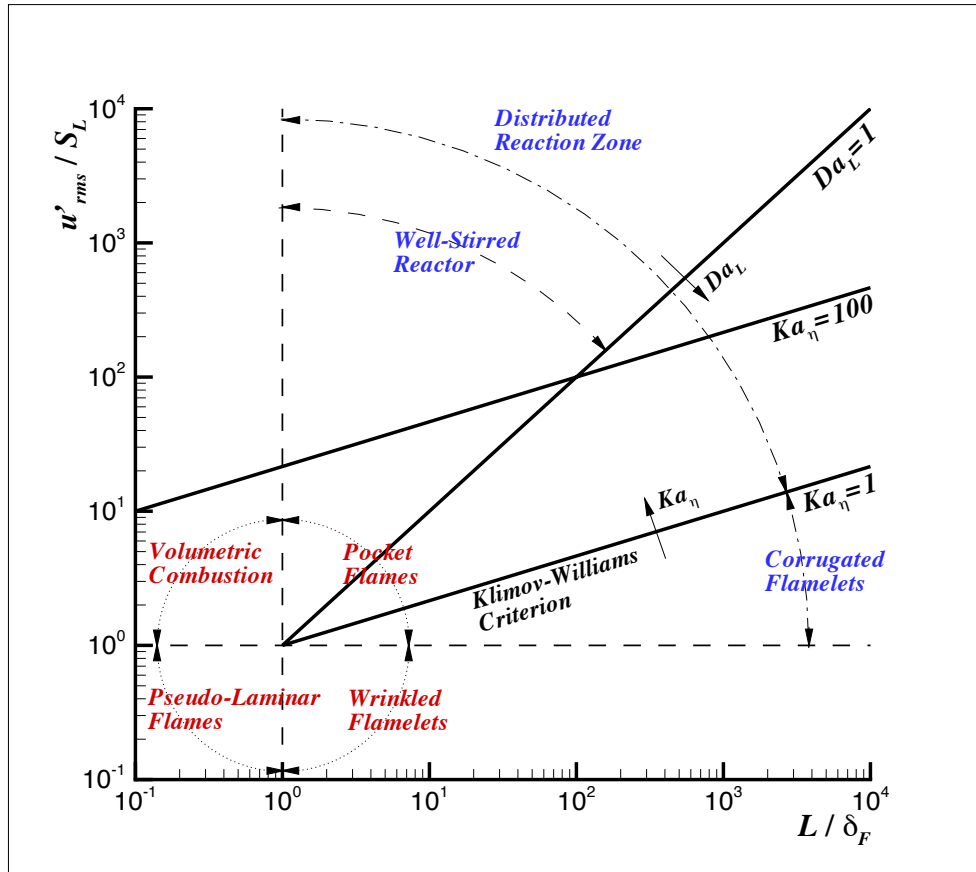
Figura 1.2: Typical combustion regime identification. The dotted arcs refer to the early definition attempt by Barrère [2]. Logarithmic scales are used for both axes. Note that the subscript ``t'' in characteristic nondimensional numbers has been avoided to simplify symbols. Note also that the maximum extension of the vertical axis is not physical.

Finally, according to the Karlovitz criterion, if $Ka_{\eta_t} > 1$ quenching occurs, i.e., no flamelet is possible. It is observed that $Ka_{\eta_t} > 1$ corresponds to $\delta_F > \eta$: so, in a $log\left(u'_{rms}/S_L\right)$ vs $log\left(L/\delta_F\right)$ plane, $Ka_{\eta_t} = 1$ corresponds to the straight line $log\left(u'_{rms}/S_L\right) = (1/3)\ log\left(L/\delta_F\right)$.

A second number, useful in evaluating the coupling between importance of turbulence and chemistry, is the turbulent Damköhler number, defined as the ratio between characteristic (convective) turbulent time and chemical time, i.e.,

$$Da_t = \frac{\tau_t}{\tau_{ch}} = \frac{L/u'_{rms}}{\delta_F/S_L} \ .$$

(1.12)

The turbulent time is assumed to be the inverse of the strain rate at the integral length scale L, and therefore, the associated Damköhler number is referred to as Da_{L_t}. When Da_{L_t} tends to infinity, chemistry is ``fast'' and the flame is passively convected by turbulence; at the opposite extreme, $Da_{L_t} \ll 1$ implies turbulence is so effective in mixing reactants to realize the so-called ``well-stirred reactor regime''. In a $log\left(u'_{rms}/S_L\right)$ vs $log\left(L/\delta_F\right)$ plane, $Da_{L_t} = 1$ corresponds to the straight line $log\left(u'_{rms}/S_L\right) = log\left(L/\delta_F\right)$.

To an order of magnitude, it is possible to define combustion regimes in a $log\left(u'_{rms}/S_L\right)$ vs $log\left(L/\delta_F\right)$ plane, as shown in Fig. 1.2, the so-called Klimov-Williams combustion diagram. An early attempt was due to Barrère [2], according to which four regimes were identified: ``pseudo-laminar flames'', ``volumetric combustion'', ``pocket flames'' and ``wrinkled flamelets''. ``Pseudo-laminar flames'' are those in the presence of very

weak turbulence ($u'_{rms}/S_L < 1$ and $L/\delta_F < 1$); ``volumetric combustion'' takes place when turbulence is so fine to promote intense mixing of reactants and distribute the reaction zone ($u'_{rms}/S_L > 1$ and $L/\delta_F < 1$); ``pocket flames'' when turbulent velocity fluctuations are intense and the integral macroscale L stretches the flame front up to the point of producing local extinction ($u'_{rms}/S_L > 1$ and $L/\delta_F > 1$); ``wrinkled flamelets'' when turbulence intensity is low and the integral macroscale wrinkles the flame front ($u'_{rms}/S_L < 1$ and $L/\delta_F > 1$), thus resulting in laminar propagation and limited turbulence - combustion interaction. This first classification can be improved by introducing the two numbers previously defined, Ka_{η_t} and Da_{L_t}. By drawing the straight line boundary $Ka_{\eta_t} = 1$, and according to the Karlovitz criterion, the ``pocket flames'' regime proposed by Barrère can be split into two new regimes: the ``corrugated flamelets'' regime ($Ka_{\eta_t} < 1$), characterized by wrinkled flame sheets with pockets of either fresh or burnt mixture surrounded by a flame front, and the ``distributed reaction zone'' regime ($Ka_{\eta_t} > 1$), where extinction happens due to stretching. The ``corrugated flamelets'' coincide with the so called ``extended flamelets''. Introducing the Damköhler number, the ``well stirred reactor'' regime can be identified within the ``distributed reaction zone'' when $Da_{L_t} < 1$. The ``well stirred reactor'' is a thickened flame regime where vortices affect both preheat and reaction zones, and the structure of the flame is not laminar.

In the identification of the ``distributed reaction zone'', the Karlovitz criterion has been used. According to this criterion, in vortex - flame interaction the dissipative scales η are responsible for the highest strain rate, but some criticism of this tenet is in order.

1. The dissipative scale η may in fact be too small to effectively stretch the flame front. This was observed by Peters [6], who proposed to shift the Karlovitz criterion from $Ka_{\eta_t} = 1$ to $Ka_{\eta_t} = 100$ [21] [22, p. 78-79]. The reason for this is that actual flames resist strain more than predicted by the Karlovitz criterion. Peters [21] considered in Eqn. (1.10) a flame reaction (kinetics-dominated) thickness $\delta_r \sim 0.1\,\delta_F$ instead of δ_F, thus obtaining the shift to $Ka_{\eta_t} = 100$. This is equivalent to say that the scale that can effectively stretch the flame front and cause extinction is larger than η. Between $Ka_{\eta_t} = 1$ and 100 vortices thicken the flame preheat zone, without altering the reaction zone that remains thin and close to a laminar reaction zone.

2. Since (Kolmogorov) $u_\eta \eta/\nu \approx 1$, viscous dissipation at η scales cannot be neglected. Thus structures at this scale will be dissipated by viscosity before they have a chance of quenching the flame.

3. Scales $l < \delta_F$ induce local high curvature, thus decreasing the effective strain. In fact, the flame stretch can be decomposed into two contributions,

$$\zeta = \nabla_t \cdot \boldsymbol{u} - S_d \nabla \cdot \boldsymbol{n}\,, \tag{1.13}$$

the first is the stretch parallel to the flame front, and the second one is related to curvature. Note that S_d is the speed at which the flame front moves along its normal, $\boldsymbol{n}$, towards the fresh mixture; in $2D$, $\nabla \cdot \boldsymbol{n}$ is the radius of curvature of flame front (usually assumed positive from fresh towards burnt gases). Therefore, for flames interacting with small vortices, curvature effects reduce flame stretch, thus counteracting the effects of high Karlovitz numbers and preventing quenching. The quenching limit $Ka_l = 1$ is valid only for large vortices, which have long lifetime and induce little flame curvature. It is observed that a consumption speed, S_c, of fresh gases through the flame front can also be defined, such that

$$\rho_u Y_R S_c = \int_{-\infty}^{+\infty} \dot{\omega} d\boldsymbol{n}\,, \tag{1.14}$$

where ρ_u and Y_R are density and mass fractions of unburnt reactants, and $\dot{\omega}$ is the consumption rate of mass reactants per unit volume and unit time. For a planar and steady laminar flame, $S_d = S_c = S_L$; for a typical natural gas Bunsen flame $S_d/S_L \sim 10$ and $S_c/S_L \sim 1$. Increasing the total flame stretch reduces flame speed. Total flame stretch is a meaningful quantity, however its estimation requires values of strain, displacement speed, and curvature. How to evaluate these quantities from an averaged description of the turbulent flow remains an open question.

Furthermore, local high curvature promote thermo-diffusive effects that oppose the influence of strain when the Lewis number of reactants is greater than one.

4. The eddy - flame front interaction is unsteady, i.e., it depends on the time-evolution of stretch and on eddy lifetime. It is observed that during flame front - vortices interaction the flame speed may decrease more slowly than the flame stretch may increase [9]; this transient dynamics features may explain why the flame still exists when the Karlovitz number is high.

5. Lastly, the eddy - flame front interaction is multi-scale, i.e., the effects on the flame front of a spectrum of length scales l, between η and L, and of a spectrum of velocity scales u'_l, with $u_\eta \leq u'_l \leq u'_{rms}$, must be considered. There are many studies about the interaction of a single vortex pair and a flame front [9]; to access the interaction between many small vortices and the flame front from these results is difficult to achieve. This issue is discussed below.

1.1.1 The Effect of Turbulent Spectra on the Klimov-Williams Diagram

From the combustion point of view, each chemical species has its own characteristic time, $\tau_{ch_i} = \rho_i/\dot{\omega}_i$, where both density and production / destruction rate depend on temperature, pressure and concentrations. A more specific definition of chemical time, associated only to the presence of a flame front, is $\tau_{ch} = \delta_F/S_L$, as already seen. This definition, adopted in combustion diagrams, does not exclude a spectrum of chemical times, since both δ_F and S_L depends on local temperature, pressure and concentrations. However, in most analyses of combustion regimes, both δ_F and S_L are implicitly assumed constant; this implies the focus is on studying the effects of turbulence on combustion, and not the vice-versa. This is a limitation of usual analyses. Furthermore, the latter definition of chemical time cannot be used when combustion is distributed, since there is no flame front; in this case a more general chemical time definition should be adopted, such as D_{mix}/S_L^2.

Knowing that there is a spectrum of turbulent scales, each point (associated to the global state of the flow) on the typical combustion diagram can be seen corresponding to a multi-scale eddy / flame interaction, to be analyzed in a spectral diagram. In a spectral diagram, the macro-turbulent scales, u'_{rms} and L, become velocity and length spectra, u'_l and l, as shown in Fig. 1.3.

In the spectral diagram of Fig. 1.3 the characteristic numbers previously defined by utilizing in some way the single macro-scale, are redefined and generalized. Thus, the ``scale'' Reynolds and Karlovitz numbers become, respectively, $Re_{l_t} = u'_l l/\nu$ and $Ka_{l_t} = (\delta_F/S_L)/\left(l/u'_l\right) \approx Re_{l_t}^{-1/2}(\delta_F/\eta)^2$. Note that at the generic scale l, the Damköhler and Karlovitz numbers have formally the same meaning since both length and velocity scales in Eqns. (1.3) and (1.12) have become the same generic length and velocity scales; in fact, $Da_l = \left(l/u'_l\right)/(\delta_F/S_L) \equiv Ka_{l_t}^{-1}$. If taken constant, these numbers on the spectral diagram are straight lines: $log\left(u'_l/S_L\right) = -log\left(l/\delta_F\right) + logRe_{l_t}$ for Re_{l_t}, and $log\left(u'_l/S_L\right) = log\left(l/\delta_F\right) + logKa_{l_t}$ for Ka_{l_t}. Also turbulent length and velocity scales lie on a straight line, $log\left(u'_l/S_L\right) = 1/3\,log\left(l/\delta_F\right) - 1/3\,logRe_{L_t} + 4/3\,log\left(u'_{rms}/S_L\right)$, that will be called ``turbulence line''. Given a turbulent flow state, defined in terms of macroscales $u'_{rms}$ and $L$ (point B), and dissipative scales $\eta$ and $u_\eta$ (point A or A'), the ``turbulence line'' is completely defined, as shown in Fig. 1.3.

Some results and observations about turbulence / combustion interaction can be discussed by reporting on the spectral diagram also the $Re_{l_t} = 1$, $Ka_{l_t} = 1$ and ``turbulence'' lines. In particular:

- dissipation takes place for $Re_{l_t} < 1$; the $Re_{l_t} = 1$ line is the locus of the dissipative scales, determined in terms of both length, η, and velocity, u_η, scales;

- quenching occurs for $Ka_{l_t} > 1$;

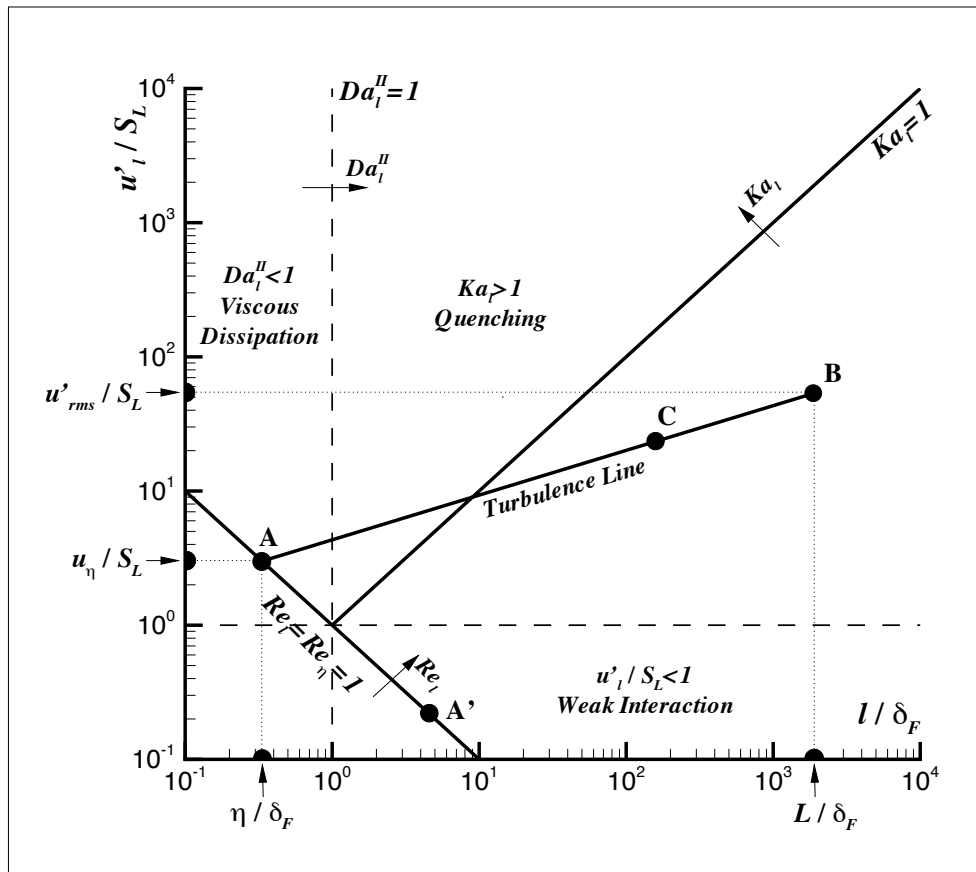- for $u'_l/S_L < 1$ the interaction is weak and no pockets form;

Figura 1.3: Spectral combustion diagram. Each point of the typical diagram in Fig. 1.2 has its own spectral diagram. Logarithmic scales are used for both axes. Note that the subscript ``t'' in characteristic nondimensional numbers has been avoided to simplify symbols.

- the ratio between the lifetime of the generic vortex of scale l, $\tau_{\nu_l} = l^2/\nu$, and the chemical time, $\tau_{ch} = \delta_F/S_L$, is the Damköhler number of second species,

$$Da_l^{II} = \frac{\tau_{\nu_l}}{\tau_{ch}} = Pr^{-1}\left(\frac{l}{\delta_F}\right)^2 \approx \left(\frac{l}{\delta_F}\right)^2 \, , \qquad (1.15)$$

having used $S_L\,\delta_F/\alpha = 1$. Similarly to the case $Re_{l_t} < 1$, eddies are destroyed by viscous dissipation before they can be convected and sustain the vortex cascade, so when $Da_l^{II} < 1$ eddies are destroyed by viscous dissipation before combustion can take place, as observed in [9]. Therefore, scales $l < \delta_F$ are dissipated and cannot interact with the flame front. From this point of view, Da_l^{II} is a measure of the generic vortex to penetrate a flame front. Furthermore, Da_l^{II} is also a good measure of curvature effects [9]. It is also observed that a vortex pair (i.e., two coherent structures with opposite signs of vorticity) has long lifetime and high power, i.e., high Da_l^{II}, thus resulting the most efficient structure in terms of flame quenching [9]. A vortex pair produces high level of stretch on its axis of simmetry, entrains the flame towards cooler gases flowing behind the flame front, thereby increasing the effects of stretch and promoting extinction.

A first conclusion is that η scales cannot quench a flame front. In fact, they lie on the $Re_{l_t} = 1$ line: in the $u_l'/S_L < 1$ region (point A') interaction is weak, even though the η scales have $Da_l^{II} > 1$; in the $l/\delta_F < 1$ region (point A) $Da_l^{II} < 1$ and η scale fluctuations ($u_l'/S_L > 1$) are dissipated by viscous effects.

Second, since the multi-scale interaction takes place along the turbulence line (segment AB or A'B), only scales within through the $Ka_{l_t} > 1$ region can quench the flame front.

These two conclusions are important in developing subgrid combustion models for LES. Given the local filter size, Δ, and its characteristic velocity, u_Δ, the generic scale (point C) is defined. This point moves along the ``turbulence'' line with changing spatial location in the computational domain. Subgrid eddies-flame interaction only takes place between points A (or A') and C ($\eta \le l_{SGS} \le \Delta$). This interaction is conditional, i.e., it takes place only if the local Reynolds number Re_Δ can produce scales in the range $[\eta, \, \Delta]$.

1.2 The Transport Equations

Gaseous combustion is governed by a set of transport equations expressing the conservation of mass, momentum and energy, and by a thermodynamic equation of state describing the gas behaviour. The derivation of these conservation equations from mass, species and energy balances may be found in standard books [1, 23, 24]. In this work, equations relying on continuum mechanics and postulating constitutive relationships are considered.

For a mixture of N_s ideal gases in local thermodynamic equilibrium and chemical nonequilibrium, the corresponding field equations (extended Navier-Stokes equations) are:

- Transport Equation of Mass

$$\frac{\partial \rho}{\partial t} + \nabla \cdot (\rho \boldsymbol{u}) = 0 \qquad (1.16)$$

- Transport Equation of Momentum

$$\frac{\partial \rho \boldsymbol{u}}{\partial t} + \nabla \cdot (\rho \boldsymbol{u} \boldsymbol{u}) = \nabla \cdot \boldsymbol{S} + \rho \sum_{i=1}^{N_s} Y_i \boldsymbol{f_i} \qquad (1.17)$$

- Transport Equation of Total Energy (internal + mechanical, $\mathcal{E} + \mathcal{K}$)

$$\frac{\partial \rho \mathcal{U}}{\partial t} + \nabla \cdot [\rho \boldsymbol{u} \mathcal{U}] = \nabla \cdot (\boldsymbol{S}\boldsymbol{u}) - \nabla \cdot \boldsymbol{q} + \rho \sum_{i=1}^{N_s} Y_i \boldsymbol{f_i} \cdot (\boldsymbol{u} + \boldsymbol{V_i}) \qquad (1.18)$$

- Transport Equation of Species Mass Fraction

$$\frac{\partial \rho Y_i}{\partial t} + \nabla \cdot (\rho \boldsymbol{u} Y_i) = -\nabla \cdot \boldsymbol{J_i} + \dot{\omega}_i \tag{1.19}$$

- Thermodynamic Equation of State

$$p = \rho \sum_{i=1}^{N_s} \frac{Y_i}{W_i} \mathcal{R}_u T \tag{1.20}$$

These equations must be coupled with the constitutive equations which describe the molecular transport properties of the flow.

In the above equations, t is the time variable, ρ the density, $\boldsymbol{u}$ the velocity, $\boldsymbol{S}$ the stress tensor, $\mathcal{U}$ the total energy per unit of mass, $\mathcal{E}$ and $\mathcal{K}$ respectively the internal and mechanical (i.e., kinetic) energies per unit of mass, $\boldsymbol{q}$ is the heat flux, p the pressure, T the temperature. For what concerns chemical species, $\boldsymbol{f_i}$ is the body force per unit of mass acting on the species i, with molecular weight W_i and mass fraction Y_i, $\dot{\omega}_i$ is the production/destruction rate of species i, diffusing at velocity $\boldsymbol{V_i}$ and resulting in a diffusive mass flux $\boldsymbol{J_i}$. Finally, $\mathcal{R}_u$ is the universal gas constant.

Summation of all species transport equations (1.19) yields the total mass conservation equation (1.16). Therefore, the N_s species transport equations (1.19) and the mass conservation equation (1.16) are linearly dependent and one of them is redundant. Furthermore, to be consistent with mass conservation, the diffusion fluxes ($\boldsymbol{J_i} = \rho Y_i \boldsymbol{V_i}$) and chemical source terms must satisfy

$$\sum_{i=1}^{N_s} \boldsymbol{J_i} = 0 \qquad and \qquad \sum_{i=1}^{N_s} \dot{\omega}_i = 0 \,. \tag{1.21}$$

In particular, the constraint on the summation of chemical source terms derives from mass conservation for each of the N_r chemical reactions of a chemical mechanism. With the tensor notation this mechanism can be written as

$$\sum_{i=1}^{N_s} \nu'_{ij} A_i = \sum_{i=1}^{N_s} \nu''_{ij} A_i \qquad with \qquad j = 1, ..., N_r \,, \tag{1.22}$$

where ν'_{ij} and ν''_{ij} are the stoichiometric coefficients of species A_i on the left ($'$) and right side ($''$) of the $j-th$ reaction. Since mass is given by the product of number of moles times molecular weight, mass conservation for each reaction, $m'_j = m''_j$, is written as

$$\sum_{i=1}^{N_s} \left(\nu''_{ij} - \nu'_{ij} \right) W_i = 0 \qquad with \qquad j = 1, ..., N_r \,. \tag{1.23}$$

The net source / sink term of the $i-th$ chemical species is

$$\dot{\omega}_i = \sum_{j=1}^{N_r} \dot{\omega}_{ij} = W_i \sum_{j=1}^{N_r} \left(\nu''_{ij} - \nu'_{ij} \right) \dot{\omega}_{Rj} \qquad with \qquad i = 1, ..., N_s \,, \tag{1.24}$$

$\dot{\omega}_{Rj}$ being the reaction rate associated to the $j-th$ reaction. Summing Eqn. (1.24) over the number of chemical species N_s,

$$\sum_{i=1}^{N_s} \dot{\omega}_i = \sum_{j=1}^{N_r} \dot{\omega}_{Rj} \sum_{i=1}^{N_s} W_i \left(\nu''_{ij} - \nu'_{ij} \right) = 0 \,, \tag{1.25}$$

after using Eqn. (1.23).

1.3 Modelling the Favre Filtered Chemical Source Term

The Favre filtered chemical source term in the energy and single species transport equations is here modelled as

$$\widetilde{\omega}_i \approx \gamma^* \omega_i^* \,, \tag{1.26}$$

γ^* and ω_i^* being the local reacting volume fraction of the computational cell and the reaction rate of the $i-th$ chemical species, respectively.

The local reacting volume fraction is defined as $\gamma^* = \mathcal{V}_{\mathcal{F}}{}^*/\mathcal{V}_\Delta$, $\mathcal{V}_{\mathcal{F}}{}^*$ and $\mathcal{V}_\Delta$ being the reacting and the total volumes of the computational cell. In particular, the suggested Localized Turbulent Scales Model (LTSM) estimates the local reacting volume fraction γ^* assuming that a flame front having a surface area $\mathcal{A}_{\mathcal{F}}$ and thickness δ_F is contained in a computational cell volume of characteristic size $\Delta = \mathcal{V}_\Delta^{1/3}$, i.e.,

$$\gamma^* = \frac{\mathcal{V}_{\mathcal{F}}{}^*}{\mathcal{V}_\Delta} \approx \frac{\mathcal{A}_{\mathcal{F}}\delta_{\mathcal{F}}}{\mathcal{V}_\Delta} \approx \frac{\mathcal{S}_{\mathcal{T}}}{\mathcal{S}_{\mathcal{L}}}\mathcal{A}_{\mathcal{L}}\frac{\delta_{\mathcal{F}}}{\mathcal{V}_\Delta} \approx \frac{\mathcal{S}_{\mathcal{T}}}{\mathcal{S}_{\mathcal{L}}}\Delta^2\frac{\delta_{\mathcal{F}}}{\Delta^3} = \frac{\mathcal{S}_{\mathcal{T}}}{\mathcal{S}_{\mathcal{L}}}\frac{\delta_{\mathcal{F}}}{\Delta} \,. \tag{1.27}$$

This expression has been obtained with two main assumptions. The first is that within a wrinkled flame front the iso-surfaces of the progress variable are parallel [25]. The second assumption is that the ratio between the turbulent and the laminar flame surface areas scales as the ratio between the associated flame speeds [1] , i.e.,

$$\frac{\mathcal{A}_{\mathcal{F}}}{\mathcal{A}_{\mathcal{L}}} \equiv \frac{\mathcal{A}_{\mathcal{T}}}{\mathcal{A}_{\mathcal{L}}} \approx \frac{\mathcal{S}_{\mathcal{T}}}{\mathcal{S}_{\mathcal{L}}} \,. \tag{1.28}$$

With this modeling, subgrid flame front wrinkling and curvature effects are synthesized in this ratio. It is reminded that the laminar flame speed can be estimated as

$$\mathcal{S}_{\mathcal{L}} \approx \left(\frac{\alpha}{\tau_{ch}}\right)^{1/2} \,, \tag{1.29}$$

the laminar flame thickness as

$$\delta_{\mathcal{L}} \approx (\alpha\,\tau_{ch})^{1/2} \,, \tag{1.30}$$

and that these two expressions imply

$$\frac{\delta_{\mathcal{L}}\,\mathcal{S}_{\mathcal{L}}}{\alpha} = 1 \,. \tag{1.31}$$

The quantity $\alpha = k/(\rho C_p)$ is the thermal diffusivity, with k being the thermal conductivity, ρ the density and C_p the specific heat at constant pressure.

It is observed that the local flame at the base of Eqn. (1.27) may be laminar or turbulent, wrinkled or not, thickened by turbulence or not, depending on the local conditions of the flow. In particular, for a local laminar (planar) flame Eqn. (1.27) reduces to $\gamma^* \approx \delta_{\mathcal{F}}/\Delta$, and this is related to a local fractal dimension of the flame front $D_3 = 2$. When combustion is locally volumetric, $\gamma^* = 1$, and this is related to a local fractal dimension of the flame front $D_3 = 3$. Equation (1.27) refers to a laminar or turbulent wrinkled flame front with $\gamma^* < 1$, and this is related to a local fractal dimension of the flame front $D_3 \in (2,3)$.

An extinction or flame stretch factor $\mathcal{G}_{ext} \leq 1$ will be introduced in Section 2.6 to take into account flame quenching due to subgrid scales. This factor has effect on γ^* that is finally given by:

$$\gamma^* = \mathcal{G}_{ext}\frac{\mathcal{S}_{\mathcal{T}}}{\mathcal{S}_{\mathcal{L}}}\frac{\delta_{\mathcal{F}}}{\Delta} \,. \tag{1.32}$$

---

[1] Alternatively, using the fractal theory, the flame front surface area could be estimated as $\mathcal{A}_{\mathcal{F}} \approx \mathcal{N}_3\,(\epsilon_{in})\,\epsilon_{in}^2$, $\mathcal{N}_3 = (\epsilon_{out}/\epsilon_{in})^{\mathcal{D}_3}$ being the number of fractal measurement cubes of size ϵ_{in} intersecting the flame front surface, ϵ_{in} being the inner cut-off length scale of the flame front surface, ϵ_{out} its outer cut-off length scale, and $\mathcal{D}_3 \in (2,3)$ its fractal dimension. Within this approach, the local reacting volume fraction is modelled as $\gamma^* \approx (\epsilon_{out}/\epsilon_{in})^{\mathcal{D}_3-2}\delta_{\mathcal{F}}/\Delta$, that, compared with Eqn. (1.27) results into the fractal assumption for the ratio between turbulent and laminar flame surface areas $\mathcal{A}_{\mathcal{T}}/\mathcal{A}_{\mathcal{L}} \approx \mathcal{S}_{\mathcal{T}}/\mathcal{S}_{\mathcal{L}} \approx (\epsilon_{out}/\epsilon_{in})^{\mathcal{D}_3-2}$. Due to the added uncertainty associated to the fractal dimension and the cut-off length scales [26], this alternative way is not preferred in this work.

The problem of γ^* estimation becomes the problem of estimating the characteristics of the local flame front in terms of its turbulent flame speed, laminar flame speed and thickness (turbulent or laminar) from the filtered conditions of the flow and depending on the related local premixed combustion regime.

The laminar quantities are estimated by means of Eqns. (1.29) and (1.30), with the local filtered chemical time given by

$$\tau_{ch} = \left(\frac{|\Delta \mathcal{H}_R|}{\rho C_p T} \right)^{-1} , \qquad (1.33)$$

where $\Delta \mathcal{H}_R = \sum_{i=1}^{N_s} \mathcal{H}_i \dot{\omega}_i$ is the heat of reaction, N_s being the number of chemical species, $\mathcal{H}_i = h_{f_i}^0(T_r) + \Delta h_{s_i}(T)$ the enthalpy of the $i - th$ chemical species, $h_{f_i}^0(T_r)$ its formation enthalpy at the reference temperature $T_r = 298.15\,\text{K}$, $\Delta h_{s_i} = \int_{T_r}^{T} C_{p_i}(T)dT$ its sensible enthalpy, and $\dot{\omega}_i$ its reaction rate.

In the following, models to derive the turbulent quantities will be proposed.

2 The Suggested Model

2.1 Vortices / Flame Front Interaction

This Section aims to answer to two fundamental questions related to the interaction problem between vortices and a flame front. What is the smallest eddy with life-time longer than the characteristic chemical time? And, then, among the surviving scales, what is the smallest eddy able to locally wrinkle a flame front? Answering to the first question lets to define the range of scales that can interact with a flame front, and eventually enter into. This will be important to model local flame thickening due to turbulence. Answering to the second question lets instead to define the smallest turbulent scales that apply the highest strain rate and curvature wrinkling onto the flame front. This will be important to model local flame quenching due to turbulence.

2.1.1 The Smallest Surviving Eddy

The interaction between a premixed flame front and eddies has been widely analyzed in literature. Results clearly show that the dissipative Kolmogorov scales η cannot quench a flame front [9]. An estimate of the smallest turbulent scale that can affect a laminar flame front without being dissipated can be obtained by considering that the turbulent $l-$scale Damköhler number of second species has to be greater than one, i.e.,

$$Da_l^{II} = \frac{\tau_{\nu_l}}{\tau_{ch}} = Pr^{-1} \left(\frac{l}{\delta_{\mathcal{L}}} \right)^2 \geq 1 \, , \tag{2.1}$$

where $\tau_{\nu_l} = l^2/\nu$ is the lifetime of the generic vortex of scale l, ν being the dynamic viscosity, $\tau_{ch} = \delta_{\mathcal{L}}/\mathcal{S}_{\mathcal{L}} = \delta_{\mathcal{L}}^2/\alpha$ is the chemical time, and $Pr = \nu/\alpha$ is the Prandtl number.

Similarly to the case $Re_l < 1$ for which eddies are destroyed by viscous dissipation before they can be convected and sustain the vortex cascade, so when $Da_l^{II} < 1$ eddies of scale l are destroyed by viscous dissipation before combustion can take place, as observed in [9]. Therefore, when $Pr = 1$ scales $l < \delta_L$ are dissipated and cannot interact with the flame front. From this point of view, Da_l^{II} is a measure of the generic vortex to penetrate a flame front. Furthermore, Da_l^{II} is also a good measure of curvature effects [9]. It is also observed that a vortex pair (i.e., two coherent structures with opposite signs of vorticity) has long lifetime and high power, i.e., high Da_l^{II}, thus resulting the most efficient structure in terms of flame quenching [9]. A vortex pair produces high level of stretch on its axis of simmetry, entrains the flame towards cooler gases flowing behind the flame front, thereby increasing the effects of stretch and promoting extinction.

These considerations, confirmed by numerical simulations and experiments, lead to conclude that the η scales cannot quench a flame front. In fact, when $u'_l/S_L < 1$ interaction is weak, even though the η scales have $Da_l^{II} > 1$; when $l/\delta_L < 1$, $Da_l^{II} < 1$ and η scale fluctuations ($u'_l/S_L > 1$) are dissipated by viscous effects (see Fig. 1.3).

Here, previous analysis is extended by removing in Eqn. (2.1) the $Pr = 1$ assumption. This is in agreement with distributions of local Prandtl number obtained from numerical simulations of different flames, as shown in Table 2.1. Hence, the smallest surviving scale l^* is estimated as

$$l^* = Pr^{1/2} \delta_{\mathcal{L}} = l_\Delta \left(Da_\Delta^I Re_\Delta \right)^{-1/2} = l_\Delta Da_\Delta^{II^{-1/2}} \, , \tag{2.2}$$

Reference	Reactants	Combustion Type	Pr Range
[27]	C_3H_8/Air	Premixed	$0.70 - 0.74$
[28]	CH_4/H_2/Air	Non-Premixed	$0.48 - 0.74$
[29]	$CO/H_2/N_2$/Air	Non-Premixed	$0.45 - 0.71$
[30]	$CO/H_2/N_2$/Air	Premixed	$0.58 - 0.71$

Tabella 2.1: Ranges of Prandtl number distributions obtained from numerical simulations of different flames.

where $Re_\Delta = u'_\Delta l_\Delta / \nu$ is the turbulent Reynolds number defined in terms of the local length[1] and velocity macroscales l_Δ and u'_Δ, $Da^I_\Delta = l_\Delta u'_\Delta / \tau_{ch}$ is the turbulent l_Δ−scale Damköhler number of first species. Turbulent scales larger than l^* will not be destroyed or damped by the flame front. It is observed that for $Pr = 1$, it is always $l^* \equiv \delta_{\mathcal{L}}$.

The smallest surviving scale $l^* \in [\eta, l_\Delta]$, and this is fulfilled for whatever Prandtl number if

$$l_\Delta \geq l^* \geq \eta \Leftrightarrow Re_\Delta^{-1} \leq Da^I_\Delta \leq Re_\Delta^{1/2} \,, \tag{2.3}$$

observing that $l^* = l_\Delta$ for $Da^I_\Delta = Re_\Delta^{-1}$ and $l^* = \eta$ for $Da^I_\Delta = Re_\Delta^{1/2}$.

An important observation is that

$$l^* \leq \delta_{\mathcal{L}} \Leftrightarrow Pr \leq 1 \,, \tag{2.4}$$

and this means that in gaseous combustion ($Pr \leq 1$) eddy-scales smaller than the flame thickness may survive and affect the flame itself, e.g., entering into it (although this has not been proved yet) and thickening it.

Another observation is that the Taylor microscale, $\lambda_g = l_\Delta \, Re_\Delta^{-1/2}$, could be used to estimate the local strain of the flow as u'_Δ / λ_g also in the eddy-flame interaction (flame strain modelling), since

$$\lambda_g \geq l^* \Leftrightarrow Da^I_\Delta \geq 1 \,. \tag{2.5}$$

The constant $\sqrt{15}$ usually present in the Taylor scale expression[2] has been here avoided since otherwise $Re_\Delta = \sqrt{15}$ would be needed to produce a local turbulent cascade with $\lambda_g = l_\Delta$. Instead, in this modelling framework a local turbulent cascade is assumed to take place for $Re_\Delta \geq 1$.

2.1.2 The Smallest Wrinkling Eddy

Looking at vortices / flame front interaction problem, some eddies will be destroyed by viscous dissipation before combustion can take place. The range of the surviving eddy-scales has been defined in Section 2.1.1. Among these scales, those smaller than the local flame front thickness, may locally enter into it and thicken it provided that $u'_\Delta \geq \mathcal{S}_{\mathcal{L}}$, u'_Δ being the local rms velocity fluctuation. However, this ``surviving'' condition is not sufficient for an eddy to locally wrinkle a flame front. Only eddies with characteristic (tangential) velocity $u'_l \geq \mathcal{S}_{\mathcal{L}}$ will be able to locally wrinkle a flame front.

Hence, given the smallest surviving eddy $l^* = l_\Delta \left(Da^I_\Delta \, Re_\Delta \right)^{-1/2}$, the smallest surviving and wrinkling eddy l^*_w will be given by the condition

$$\frac{u'_{l^*}}{\mathcal{S}_{\mathcal{L}}} \geq 1 \Rightarrow \frac{u'_\Delta}{\mathcal{S}_{\mathcal{L}}} \left(\frac{l^*}{l_\Delta} \right)^{1/3} = Pr^{1/2} \left(Re_\Delta Da^{I-2}_\Delta \right)^{1/3} \geq 1 \,. \tag{2.6}$$

---

[1]A good question is how the local length macroscale could be estimated. It could be estimated via the subgrid kinetic energy and its dissipation rate, each one requiring its own transport equation. Otherwise, it would not be possible to define $l_\Delta > \Delta$ (Δ being the computational cell size). The only remaining assumption is $l_\Delta \equiv \Delta$.

[2]The (transversal) Taylor microscale λ_g is the turbulent length scale mainly used by experimentalists to characterize the mean spatial extension of the velocity gradients. This scale is defined in the framework of isotropic turbulence as the scale associated to the dissipation $\varepsilon = 15\nu \overline{u^2_{,x}}$ and obtained via dimensional analysis, i.e., $\lambda^2_g \approx \overline{u'^2}/\overline{u^2_{,x}}$. Hence, $\varepsilon \approx 15\nu \overline{u'^2}/\lambda^2_g$. Considering the conservation of ε along the inertial turbulence cascade, i.e., $15\nu \overline{u'^2}/\lambda^2_g = \overline{u'^3}/L_t$, the expression $\lambda_g \approx \sqrt{15} L_t \, Re_{L_t}^{-1/2}$ is finally obtained, L_t being the integral macroscale and u' its characteristic velocity fluctuation (rms).

Regime	Scale Condition		Da_Δ^I Condition
$\mathcal{V_R}$	$\delta_\mathcal{L} \geq l_\Delta$	$\Rightarrow$	$Da_\Delta^I \leq Pr^{-1}Re_\Delta^{-1}$
$\mathcal{TTC_R}$	$l_\Delta > \delta_\mathcal{L} \geq \eta$	$\Rightarrow$	$Pr^{-1}Re_\Delta^{1/2} \geq Da_\Delta^I > Pr^{-1}Re_\Delta^{-1}$
$\mathcal{W_R}$	$\delta_\mathcal{L} < \eta$	$\Rightarrow$	$Da_\Delta^I > Pr^{-1}Re_\Delta^{1/2}$

Tabella 2.2: The three main premixed combustion regimes based on the comparison between turbulent length scales and laminar flame front thickness.

This means that the surviving scales l^* become l_w^*, i.e., able to locally wrinkle a flame front if

$$Da_\Delta^I \leq Pr^{3/4}Re_\Delta^{1/2} \, . \tag{2.7}$$

This condition in terms of the Karlovitz numbers defined in Section 2.6 becomes:

$$Ka_{l^*} = Ka_\eta^{2/3} \equiv Ka_{\lambda_g}^{2/3} \geq Pr^{-1/2} \, . \tag{2.8}$$

Substituting the maximum Damköhler number for the smallest surviving and wrinkling scale given by Eqn. (2.7) into Eqn. (2.2), the minimum surviving and wrinkling scale l_w^* is obtained:

$$l_w^*|_{min} = Pr^{-3/8}\eta \geq \eta \, . \tag{2.9}$$

Hence, it is observed that l_w^* decreases as $l_\Delta \left(Da_\Delta^I \, Re_\Delta \right)^{-1/2}$ by increasing Da_Δ^I up to $Da_\Delta^I = Pr^{3/4}Re_\Delta^{1/2}$. Then, l_w^* maintains its minimum value $Pr^{-3/8}\eta$ for whatever $Da_\Delta^I \geq Pr^{3/4}Re_\Delta^{1/2}$, implying that the highest local flame front curvature can be $2\,l_w^{*-1} = 2\,Pr^{3/8}/\eta$.

From what found above, the minimum scale Reynolds number for flame front wrinkling will be

$$Re_{l_w^*}\big|_{min} = \frac{\mathcal{S_L}\,l^*}{\nu} \equiv \frac{\mathcal{S_L}\,l_w^*|_{min}}{\nu} = Pr^{-1/2} \geq 1 \, . \tag{2.10}$$

It is observed that simple chemistry DNS calculations [9, 31] showed

$$\frac{l_w^*|_{min}}{\delta_\mathcal{L}} = 0.2 + 5.5 \left(\frac{\varepsilon\delta_\mathcal{L}}{\mathcal{S_L}^3} \right)^{-1/6} \Rightarrow Re_{l_w^*}\big|_{min} \approx 5.5^{3/2}\,Da_l^{I-1/2}\,Pr^{-1} \, , \tag{2.11}$$

with $\varepsilon = u_l'^3/l$. Experimental work [32, 33] instead showed

$$\frac{u_{l^*}'\big|_{min}}{\mathcal{S_L}} = 2.5 \left(\frac{l_w^*|_{min}}{\delta_\mathcal{L}} \right)^{-1} \Rightarrow Re_{l_w^*}\big|_{min} \approx 2.5\,Pr^{-1} \, . \tag{2.12}$$

Large differences are expected between experiments, simple chemistry DNS calculations and theoretical results. However, the trends of these three different approaches are qualitatively well reproduced, looking at the $Re_{l_w^*}\big|_{min} = f\left(Pr \right)$ dependence.

2.2 Premixed Combustion Regimes

Thinking to the interaction between a flame front and turbulent eddies, it is possible to identify three main combustion regimes based on the comparison between the local laminar flame front $\delta_\mathcal{L}$, the local turbulent macro-scale l_Δ, and the local turbulent dissipative scale η. These regimes are described in Table 2.2 and they are named, rispectively, $\mathcal{V_R}$ from $\mathcal{Volumetric\,Regime}$, $\mathcal{TTC_R}$ from $\mathcal{Thickened,\,Turbulence-Thickened,\,Corrugated\,Regimes}$, $\mathcal{W_R}$ from $\mathcal{Wrinkled\,Regime}$.

2.3 The $\mathcal{T}$urbulence-$\mathcal{T}$hickened $\mathcal{R}$egime: the Zimont Model

In Section 2.1.1 it was shown that some scales smaller than the flame thickness may not be dissipated. These scales may affect the flame front itself thickening it but leaving unchanged the chemical time: this is the base of Zimont's model [34, 35, 36]. The thickening process can be modelled via a turbulent thermal diffusivity $\alpha^* \approx u^* l_{tk}^*$, u^* being the characteristic velocity of the scale $l_{tk}^* \approx u^* \tau_{ch}$ that is the survived and thickening turbulent scale obtained via Eqn. (2.1) with a turbulent viscosity $\nu^* \approx u^* l_{tk}^*$. With these assumptions the thickened flame front $\delta_{\mathcal{F}}^*$ can be estimated as

$$\delta_{\mathcal{F}}^* \approx (\alpha^* \tau_{ch})^{1/2} \approx (u^* l_{tk}^* \tau_{ch})^{1/2} \approx u^* \tau_{ch} \approx l_\Delta Da_\Delta^{I-3/2} \;, \tag{2.13}$$

having obtained u^* via the turbulence energy cascade, $u^* \approx u_\Delta' (l_{tk}^*/l_\Delta)^{1/3} \approx u_\Delta' Da_\Delta^{I-1/2}$. It is observed that l_{tk}^* has to be larger than l^* given by Eqn. (2.2) and, in particular, it comes out $l_{tk}^* \equiv \delta_{\mathcal{F}}^*$. The same result for $\delta_{\mathcal{F}}^*$ is obtained, as in Zimont's model [34, 36], by assuming $\alpha^* \approx u^* l_{tk}^* \approx u^* \delta_{\mathcal{F}}^*$, i.e., that the smallest surviving scale is of the order of the thickened flame front.

From Eqn. (2.13) the laminar thickened flame speed is

$$\mathcal{S_L}^* \approx \left(\frac{\alpha^*}{\tau_{ch}} \right)^{1/2} \approx \left(\frac{u^* \delta_{\mathcal{F}}^*}{\tau_{ch}} \right)^{1/2} \approx u_\Delta' Da_\Delta^{I-1/2} \equiv u^* \;. \tag{2.14}$$

From Eqn. (1.28) and assuming the ratio between the turbulent and laminar flame surface areas, $\mathcal{A_T}/\mathcal{A_L} \approx Da_\Delta^{I3/4}$ [34, 36], the turbulent tickened flame speed can be scaled as

$$\mathcal{S_T}|_{\mathcal{Z}} \approx \mathcal{A_Z} \mathcal{S_L}^* \frac{\mathcal{A_T}}{\mathcal{A_L}} \approx \mathcal{A_Z} \mathcal{S_L}^* Da_\Delta^{I3/4} \approx \mathcal{A_Z} u_\Delta' Da_\Delta^{I1/4} \;, \tag{2.15}$$

$\mathcal{A_Z} = 0.5$ being an empirical constant [35, 37]. If the constant $\mathcal{A_Z}$ is introduced in Eqn. (2.15), it has to be put also in Eqn. (2.14), and then in Eqn. (2.13), i.e.,

$$\delta_{\mathcal{F}}^* \approx \mathcal{A_Z} l_\Delta Da_\Delta^{I-3/2} \;, \tag{2.16}$$

to keep the chemical time constant.

In terms of nondimensional Prandtl and turbulent Reynolds numbers, $\mathcal{S_T}/\mathcal{S_L}|_{\mathcal{Z}}$ becomes

$$\left. \frac{\mathcal{S_T}}{\mathcal{S_L}} \right|_{\mathcal{Z}} \approx \mathcal{A_Z} \left(Pr Re_\Delta \right)^{1/2} Da_\Delta^{I-1/4} \;. \tag{2.17}$$

Assuming the chemical time unchanged, the thickness of the turbulent flame front is

$$\delta_{\mathcal{F}}^{\mathcal{T}}|_{\mathcal{Z}} \approx \mathcal{S_T}|_{\mathcal{Z}} \tau_{ch} \approx \mathcal{A_Z} l_\Delta Da_\Delta^{I-3/4} \;, \tag{2.18}$$

so that $\delta_{\mathcal{F}}^{\mathcal{T}} / \left. \mathcal{S_T} \right|_{\mathcal{Z}} = \tau_{ch}$.

2.3.1 Range of the $\mathcal{T}$urbulence-$\mathcal{T}$hickened $\mathcal{R}$egime

Imposing the conditions reported in Table 2.3, the $\mathcal{T}$urbulence - $\mathcal{T}$hickened flame $\mathcal{R}$egime validity ranges are obtained in terms of the local Damköhler number, Da_Δ^I. These ranges are reported in Table 2.4.

It is observed that gaseous combustion has $Pr < 1$, and hence, in this case it is only the $\mathcal{Z}2$ regime to be considered. The condition $Pr \geq 1$ can take place in supercritic gaseous flows, where gases has molecular transport properties more similar to liquids. However, also in these flows the Prandtl number turns back lower than one very quickly when the supercritic cold flow is preheated approaching the reacting zone. This means that the generalized subgrid combustion model that is proposed in this article can also be used in supercritic reacting flows.

The expressions for the laminar and turbulent flame thickness associated to the three boundaries of the validity ranges shown in Table 2.4 are reported in Table 2.5.

List	Condition	Type of Condition		Range
1	$\delta_{\mathcal{L}} \leq l_{\Delta}$	subgrid modelling 1	$\Rightarrow$	$Da_{\Delta}^{I} \geq Pr^{-1}Re_{\Delta}^{-1}$
2	$\delta_{\mathcal{L}} \geq \eta$	minimum thickening	$\Rightarrow$	$Da_{\Delta}^{I} \leq Pr^{-1}Re_{\Delta}^{1/2}$
3	$\delta_{\mathcal{F}}^{*} \geq \delta_{\mathcal{F}}$	thickening effect 1	$\Rightarrow$	$Da_{\Delta}^{I} \leq Pr^{1/2}Re_{\Delta}^{1/2}$
4	$\delta_{\mathcal{F}}^{\mathcal{T}} \geq \delta_{\mathcal{F}}^{*}$	thickening effect 2	$\Rightarrow$	$Da_{\Delta}^{I} \geq 1$
5	$\delta_{\mathcal{F}}^{\mathcal{T}} \leq l_{\Delta}$	subgrid modelling 2	$\Rightarrow$	$Da_{\Delta}^{I} \geq 1$
6	$l_{tk}^{*} \geq l^{*}$	minimum scale	$\Rightarrow$	$Da_{\Delta}^{I} \leq Re_{\Delta}^{1/2}$
7	$u_{\Delta}' \geq \mathcal{S}_{\mathcal{L}}$	velocity fluctuation	$\Rightarrow$	$Da_{\Delta}^{I} \leq Pr^{-1}Re_{\Delta}$

Tabella 2.3: Conditions applied to determine the validity range of the $\mathcal{T}urbulence$-$\mathcal{T}hickened$ flame $\mathcal{R}egime$.

Range	Pr Condition		Da_{Δ}^{I} Condition
$\mathcal{Z}1$	$Re_{\Delta}^{1/2} \geq Pr \geq 1$	$\Rightarrow$	$Pr^{-1}Re_{\Delta}^{1/2} \geq Da_{\Delta}^{I} \geq 1$
$\mathcal{Z}2$	$1 \geq Pr \geq Re_{\Delta}^{-1}$	$\Rightarrow$	$Pr^{1/2}Re_{\Delta}^{1/2} \geq Da_{\Delta}^{I} \geq 1$

Tabella 2.4: Validity ranges of the $\mathcal{T}urbulence$-$\mathcal{T}hickened$ flame $\mathcal{R}egime$.

The expression for the local reacting volume fraction γ^{*}, Eqn. (1.32), in the turbulent thickened flame regime becomes:

$$\gamma^{*} = \mathcal{G}_{ext} \frac{\mathcal{S}_{\mathcal{T}}}{\mathcal{S}_{\mathcal{L}}} \frac{\delta_{\mathcal{F}}}{\Delta} = \mathcal{G}_{ext} \left. \frac{\mathcal{S}_{\mathcal{T}}}{\mathcal{S}_{\mathcal{L}}} \right|_{\mathcal{Z}} \frac{\delta_{\mathcal{F}}^{*}}{\Delta} , \qquad (2.19)$$

with $\mathcal{S}_{\mathcal{T}}/\mathcal{S}_{\mathcal{L}}|_{\mathcal{Z}}$ and $\delta_{\mathcal{F}}^{*}$ given by Eqns. (2.15) and (2.16). Without considering the effect of $\mathcal{G}_{ext}$, i.e., assuming $\mathcal{G}_{ext} = 1$ in Eqn. (2.19), the volume fraction γ^{*} has to be less than one. This condition increases the lower limit of the $\mathcal{T}urbulence$-$\mathcal{T}hickened$ flame $\mathcal{R}egime$, as shown in Tables 2.6 and 2.7.

2.4 A Closer Look to Premixed Combustion Regimes

The premixed combustion regimes described in Section 2.2 are here analysed in more details considering the model developed in Section 2.3. In particular, depending on the local Prandtl number, there can be four possible conditions, as shown in Table 2.8.

Looking at Table 2.1 that reports some examples of Prandtl number ranges for gaseous combustion, among the five groups of turbulent combustion regimes described in Table 2.8, the second one ($1 \geq Pr \geq Re_{\Delta}^{-1}$) is the most physical ($Pr^{-1} = 0.5$ and 0.33 at $Re_{\Delta} = 2$ and 3, respectively). Hence, this is the sole group that will be considered in detail and used to develop a subgrid turbulent combustion closure for the chemical source rate. This assumption implies that the subgrid scale model for turbulence / combustion interaction would be switched on for $Re_{\Delta} \geq Pr^{-1}$, being $Pr \leq 1$ ($Re_{\Delta} \geq 1.35$ and 2.22 at $Pr = 0.74$ and 0.45, respectively, considering the extreme values in Table 2.1). For $Re_{\Delta} < Pr^{-1}$ the subgrid flame would be considered locally laminar. However, another assumption will be here taken, furtherly increasing the activation cell Reynolds number.

Considering the smallest surviving and wrinkling scale l_{w}^{*} defined in Section 2.1.2, it is observed that the minimum scale Reynolds number for flame front wrinkling is $Re_{l^{*}}|_{min} = Pr^{-1/2}$, as shown in Eqn. (2.10). Hence, this will be also the minimum computational cell Reynolds number to switch the subgrid turbulent combustion model on (this is guaranteed since the model is activated at least for $Re_{\Delta} \geq Pr^{-1}$. At $Da_{\Delta}^{I}|_{l_{w,min}^{*}} = Pr^{3/4}Re_{\Delta}^{1/2}$, the scale l_{w}^{*} reaches its minimum value $Pr^{-3/8}\eta$, maintained for whatever $Da_{\Delta}^{I} \geq Pr^{3/4}Re_{\Delta}^{1/2}$. For $1 \geq Pr \geq Re_{\Delta}^{-1}$ this particular Da_{Δ}^{I} is located as: $(PrRe_{\Delta})^{1/2} \geq Da_{\Delta}^{I}|_{l_{w,min}^{*}} \geq (PrRe_{\Delta})^{2/7}$ for $1 \geq Pr \geq Re_{\Delta}^{-6/13}$, and $(PrRe_{\Delta})^{2/7} > Da_{\Delta}^{I}|_{l_{w,min}^{*}} > 1$ for $Re_{\Delta}^{-6/13} > Pr \geq Re_{\Delta}^{-1}$. Note that for

Da_Δ^I	τ_{ch}	δ_L	$\delta_{\mathcal{F}}^{\mathcal{T}}$
1	l_Δ/u'_Δ	$l_\Delta\left(PrRe_\Delta\right)^{-1/2}$	l_Δ
$Pr^{-1}Re_\Delta^{1/2}$	$PrRe_\Delta^{-1/2}l_\Delta/u'_\Delta$	η	$Pr^{3/4}\left(l_\Delta\eta\right)^{1/2}$
$Pr^{1/2}Re_\Delta^{1/2}$	$\left(PrRe_\Delta\right)^{-1/2}l_\Delta/u'_\Delta$	$l_\Delta\left(PrRe_\Delta\right)^{-3/4}$	$Pr^{-3/8}\left(l_\Delta\eta\right)^{1/2}$

Tabella 2.5: Chemical time, laminar and turbulent flame thickness at the Da_Δ^I boundaries of the $\mathcal{T}urbulence\text{-}\mathcal{T}hickened$ flame $\mathcal{R}egime$ reported in Table 2.4.

List	Condition	Type of Condition		Range
8	$\frac{\mathcal{S}_\mathcal{T}}{\mathcal{S}_\mathcal{L}}\frac{\delta_{\mathcal{F}}^*}{\Delta}\leq 1$	reacting volume fraction	$\Rightarrow$	$Da_\Delta^I \geq Pr^{2/7}Re_\Delta^{2/7}$

Tabella 2.6: New condition applied to determine the validity range of the $\mathcal{T}urbulence\text{-}\mathcal{T}hickened$ flame $\mathcal{R}egime$.

$Pr = Re_\Delta^{-6/13}$, it is $Da_\Delta^I\big|_{l^*_{w,min}} \equiv (PrRe_\Delta)^{2/7}$, i.e., meaning that it is located at the lower boundary of the $\mathcal{T}urbulence\text{-}\mathcal{T}hickened\ \mathcal{R}egime$.

In order to have a sufficiently high minimum cell Reynolds number to guarantee a minimum subgrid turbulence / combustion interaction, it is here assumed to increase the activation cell Reynolds number by considering only the range $1 \geq Pr \geq Re_\Delta^{-6/13}$ for the subgrid scale turbulent combustion model. This assumption implies that the subgrid scale model for turbulence / combustion interaction will be switched on for $Re_\Delta \geq Pr^{-13/6}$, being $Pr \leq 1$ ($Re_\Delta \geq 1.92$ and 5.64 at $Pr = 0.74$ and 0.45, respectively, considering the extreme values in Table 2.1). For $Re_\Delta < Pr^{-13/6}$ the subgrid flame will be considered locally laminar.

Details about the selected group of turbulent combustion regimes with the validity range $1 \geq Pr \geq Re_\Delta^{-6/13}$ are provided in Fig. 2.1. It is observed that all the information in this figure are also valid for $1 \geq Pr \geq Re_\Delta^{-1}$, apart from the location of the $Da_\Delta^I\big|_{l^*_{w,min}}$. In particular, this figure shows the ranges of the combustion regimes and the ordered list of the main scales of turbulence and combustion. Specific values of some scales are also highlighted, as well as the ranges affected by the extinction or flame stretch factor $\mathcal{G}_{ext}$ introduced in Section 2.6. In the same figure, it is also evidenced that if $Pr = 1$ or $Pr = Re_\Delta^{-1}$, some regimes collapse. In particular, if $Pr = 1$ the $\mathcal{C}orrugated\ \mathcal{R}egime$ disappears, and in the $\mathcal{V}olumetric\ \mathcal{R}egime$ it is always $l^* > l_\Delta$. If $Pr = Re_\Delta^{-1}$ the $\mathcal{T}hickened$ and $\mathcal{T}urbulence\text{-}\mathcal{T}hickened\ \mathcal{R}egimes$ disappear (however, this can not happen due to the limiting assumption $1 \geq Pr \geq Re_\Delta^{-6/13}$).

2.5 Modelling the Reacting Volume Fraction

The reacting volume fraction γ^* in Eqn. (1.27) will have to be modelled differently depending on the combustion regimes shown in Fig. 2.1. In this Section the effect of quenching due to turbulent scales, i.e., the $\mathcal{G}_{ext}$ function, is not taken into account. Hence, attention is posed on

$$\gamma^* = \frac{\mathcal{S}_\mathcal{T}}{\mathcal{S}_\mathcal{L}}\frac{\delta_\mathcal{F}}{\Delta}\ . \tag{2.20}$$

For subgrid turbulent combustion, i.e., $Re_\Delta \geq Pr^{-1}$, with $Pr \leq 1$, γ^* is modelled as

- $\mathcal{V}olumetric\ \mathcal{R}egime$

$$\gamma^* = 1 \tag{2.21}$$

Range	Pr Condition		Da_Δ^I Condition
$\mathcal{Z}1_N$	$Re_\Delta^{1/6} \geq Pr \geq 1$	$\Rightarrow$	$Pr^{-1}Re_\Delta^{1/2} \geq Da_\Delta^I \geq Pr^{2/7}Re_\Delta^{2/7}$
$\mathcal{Z}2_N$	$1 \geq Pr \geq Re_\Delta^{-1}$	$\Rightarrow$	$Pr^{1/2}Re_\Delta^{1/2} \geq Da_\Delta^I \geq Pr^{2/7}Re_\Delta^{2/7}$

Tabella 2.7: New validity ranges of the $\mathcal{T}urbulence$-$\mathcal{T}hickened$ flame $\mathcal{R}egime$. Between the two possible ranges, the one related to gaseous combustion (also in supercritical conditions) is the second one, $\mathcal{Z}2_N$, characterized by $Pr \leq 1$.

- $\mathcal{T}hickened$ $\mathcal{R}egime$

$$\gamma^* = \frac{\delta_\mathcal{L}}{\Delta} = \left(Pr\, Re_\Delta\, Da_\Delta^I\right)^{-1/2} \leq 1 \tag{2.22}$$

$$\gamma^*|_{max} = 1 \qquad \gamma^*|_{min} = (Pr\, Re_\Delta)^{-9/14} \leq 1$$

- $\mathcal{T}urbulence$-$\mathcal{T}hickened$ $\mathcal{R}egime$

$$\gamma^* = \left.\frac{\mathcal{S}_\mathcal{T}}{\mathcal{S}_\mathcal{L}}\right|_\mathcal{Z} \frac{\delta_\mathcal{F}^*}{\Delta} = \mathcal{A}_\mathcal{Z}\left(Pr\, Re_\Delta\, Da_\Delta^{I-7/2}\right)^{1/2} < 1 \tag{2.23}$$

$$\gamma^*|_{max} = \mathcal{A}_\mathcal{Z} < 1 \qquad \gamma^*|_{min} = \mathcal{A}_\mathcal{Z}\left(Pr\, Re_\Delta\right)^{-3/8} < 1$$

- $\mathcal{C}orrugated$ $\mathcal{R}egime$

$$\gamma^* = \left.\frac{\mathcal{S}_\mathcal{T}}{\mathcal{S}_\mathcal{L}}\right|_\mathcal{C} \frac{\delta_\mathcal{L}}{\Delta} \approx \left.\frac{\mathcal{S}_\mathcal{T}}{\mathcal{S}_\mathcal{L}}\right|_\mathcal{Z} \frac{\delta_\mathcal{L}}{\Delta} = \mathcal{A}_\mathcal{Z}Da_\Delta^{I-3/4} < 1 \tag{2.24}$$

$$\gamma^*|_{max} = \mathcal{A}_\mathcal{Z}\left(Pr\, Re_\Delta\right)^{-3/8} < 1 \qquad \gamma^*|_{min} = \mathcal{A}_\mathcal{Z}\left(Pr^{-2}\, Re_\Delta\right)^{-3/8} < 1$$

having used the Zimont expression for $\mathcal{S}_\mathcal{T}$ also in this regime due to the lack of reliable experimental data [37] and the superiority of Zimont model with respect to other models [37];

- $\mathcal{W}rinkled$ $\mathcal{R}egime$

$$\gamma^* = \left.\frac{\mathcal{S}_\mathcal{T}}{\mathcal{S}_\mathcal{L}}\right|_\mathcal{W} \frac{\delta_\mathcal{L}}{\Delta} \approx \frac{\delta_\mathcal{L}}{\Delta} = \left(Pr\, Re_\Delta\, Da_\Delta^I\right)^{-1/2} \leq 1 \tag{2.25}$$

$$\gamma^*|_{max} = Re_\Delta^{-3/4} = \frac{\eta}{l_\Delta} \leq 1 \qquad \gamma^*|_{min} \to 0$$

having neglected, for the time being, subgrid hydrodynamic effects and Lewis number effects on $\mathcal{S}_\mathcal{T}$. However, it is observed that this regime appears to be of minor importance to industrial applications [37].

Work is currently going on by the present authors to define, in this low strain regime (Markstein regime), an $\mathcal{X}$ factor taking into account thermo-diffusive effects (induced by reactants' Lewis number) that increase or decrease the turbulent flame speed and flame wrinkling: $\mathcal{S}_\mathcal{T}/\mathcal{S}_\mathcal{L} = 1 - \mathcal{X}$, with $\mathcal{X} > 0$ or $\mathcal{X} < 0$ depending on local curvature, strain and Markstein number signs.

It is observed that $\Delta \equiv l_\Delta$ was assumed in deriving the non-dimensional number dependence in previous expressions, and that all of them guarantee $\gamma^* \leq 1$.

For subgrid laminar or pseudo-laminar combustion, i.e., $Re_\Delta < Pr^{-13/6}$, γ^* is modelled as

- $\mathcal{L}aminar$ $\mathcal{V}olumetric$ $\mathcal{R}egime$ ($\delta_\mathcal{L} \geq \Delta$)

$$\gamma^* = 1 \tag{2.26}$$

- $\mathcal{L}aminar$ (Planar) $\mathcal{F}lamelet$ $\mathcal{R}egime$ ($\delta_\mathcal{L} < \Delta$)

$$\gamma^* = \frac{\delta_\mathcal{L}}{\Delta} < 1\,. \tag{2.27}$$

$Re_\Delta^{-1} \geq Pr$		
$\mathcal{V_R}$	$\mathcal{TTC_R}$	$\mathcal{W_R}$
$Da_\Delta^I \leq (PrRe_\Delta)^{-1}(\geq 1)$	$Pr^{-1}Re_\Delta^{1/2} \geq Da_\Delta^I \geq (PrRe_\Delta)^{-1}$	$Da_\Delta^I \geq Pr^{-1}Re_\Delta^{1/2}$

$1 \geq Pr \geq Re_\Delta^{-1}$		
$\mathcal{V_R}$	$\mathcal{TTC_R}$	$\mathcal{W_R}$
$Da_\Delta^I \leq (PrRe_\Delta)^{-1}(\leq 1)$	$Pr^{-1}Re_\Delta^{1/2} \geq Da_\Delta^I \geq (PrRe_\Delta)^{-1}$ $\mathcal{Z}2_N \subset \mathcal{TTC_R}$ $(PrRe_\Delta)^{1/2} \geq Da_\Delta^I \geq (PrRe_\Delta)^{2/7}$	$Da_\Delta^I \geq Pr^{-1}Re_\Delta^{1/2}$

$Re_\Delta^{1/6} \geq Pr \geq 1$		
$\mathcal{V_R}$	$\mathcal{TTC_R}$	$\mathcal{W_R}$
$Da_\Delta^I \leq (PrRe_\Delta)^{-1}(\leq 1)$	$Pr^{-1}Re_\Delta^{1/2} \geq Da_\Delta^I \geq (PrRe_\Delta)^{-1}$ $\mathcal{Z}1_N \subset \mathcal{TTC_R}$ $Pr^{-1}Re_\Delta^{1/2} \geq Da_\Delta^I \geq (PrRe_\Delta)^{2/7}$	$Da_\Delta^I \geq Pr^{-1}Re_\Delta^{1/2}$

$Re_\Delta^{1/2} \geq Pr \geq Re_\Delta^{1/6}$		
$\mathcal{V_R}$	$\mathcal{TTC_R}$	$\mathcal{W_R}$
$Da_\Delta^I \leq (PrRe_\Delta)^{-1}(\leq 1)$	$Pr^{-1}Re_\Delta^{1/2} \geq Da_\Delta^I \geq (PrRe_\Delta)^{-1}$	$Da_\Delta^I \geq Pr^{-1}Re_\Delta^{1/2}$

$Pr \geq Re_\Delta^{1/2}$		
$\mathcal{V_R}$	$\mathcal{TTC_R}$	$\mathcal{W_R}$
$Da_\Delta^I \leq (PrRe_\Delta)^{-1}(\leq 1)$	$(1 \geq)Pr^{-1}Re_\Delta^{1/2} \geq Da_\Delta^I \geq (PrRe_\Delta)^{-1}$	$Da_\Delta^I \geq Pr^{-1}Re_\Delta^{1/2}$

Tabella 2.8: Ranges of the premixed turbulent combustion regimes. The most likely to happen in gaseous combustion (also in supercritical condition) is the second one, $1 \geq Pr \geq Re_\Delta^{-1}$.

2.6 The Extinction Factor

Turbulent eddies can stretch a flame front up to local quenching. Hence, considering this effect in modeling turbulent premixed flames is mandatory. In literature there are already some models for quenching. Here, a couple of them are highlighted and one chosen to estimate the extinction or stretch factor $\mathcal{G}_{ext} \leq 1$ in Eqn. (1.32).

It is observed that when $\mathcal{G}_{ext} = 1$ at subgrid level does not imply that stretching is not experienced by the flame at all. It means that the subgrid turbulence is so weak not to effectively stretch the subgrid flamelets, but the resolved velocity fluctuations may be high enough to effectively stretch the resolved flame front.

2.6.1 Bray's Stretch Factor

An extinction or stretch factor $\mathcal{G}_{ext}\left(g_{cr}\tau_\eta\right) \leq 1$ was firstly introduced by Bray [38], then adopted in models [35, 36, 39]:

$$\mathcal{G}_{ext}\left(g_{cr}\tau_\eta\right) = \frac{1}{2}erfc\left[\frac{-2\,ln\left(g_{cr}\tau_\eta\right) + \sigma^2/2}{\sqrt{2}\sigma}\right] = \tag{2.28}$$

$$= \frac{1}{2}erfc\left\{-\left(\frac{1}{2\sigma}\right)^{1/2}\left[ln\left(\frac{\varepsilon_{cr}}{\varepsilon}\right) + \frac{\sigma}{2}\right]\right\}.$$
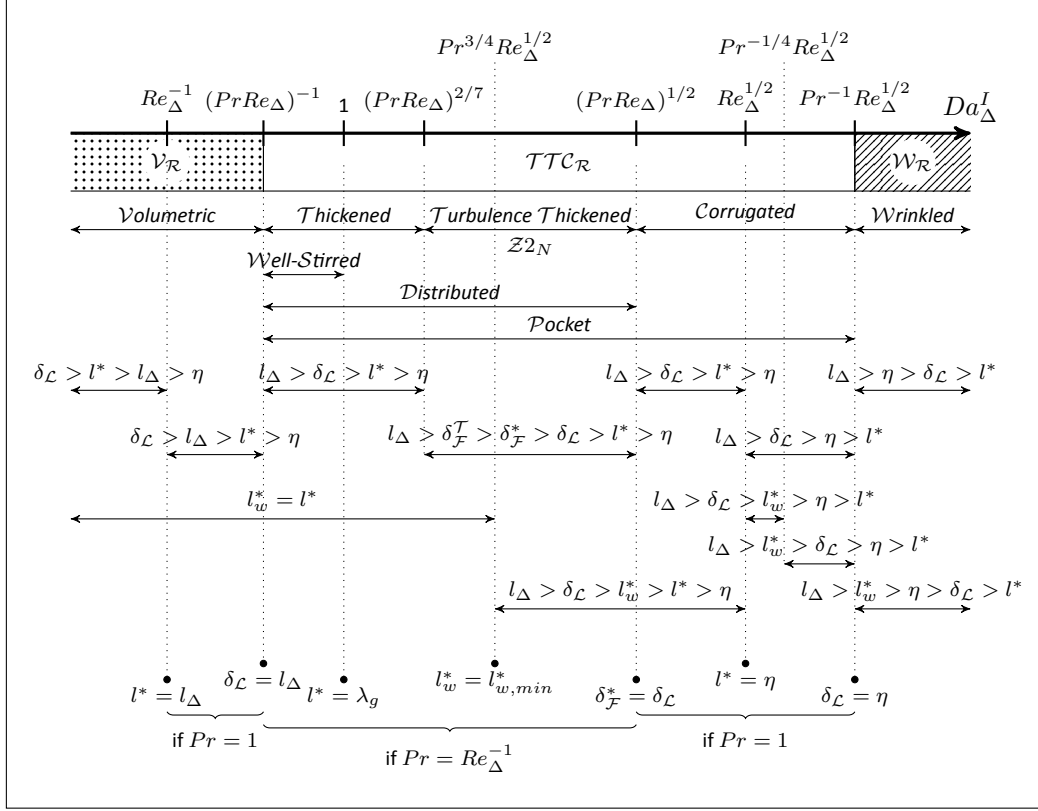
Figura 2.1: Description of the turbulent combustion regimes for $1 \geq Pr \geq Re_{\Delta}^{-6/13}$, i.e., for $Re_{\Delta} \geq Pr^{-13/6}$, with $Pr \leq 1$. Main scales of turbulence and combustion are also compared and ordered. Note that information in this figure are also valid for $1 \geq Pr \geq Re_{\Delta}^{-1}$, apart from the location of $Da_{\Delta}^{I}|_{l_{w,min}^{*}} = Pr^{3/4}Re_{\Delta}^{1/2}$ that would be located between 1 and $(PrRe_{\Delta})^{2/7}$ for $Re_{\Delta}^{-6/13} > Pr \geq Re_{\Delta}^{-1}$.

In this expression $erfc$ is the complementary error function, $\tau_{\eta} = (\nu_u/\varepsilon)^{1/2}$ is the Kolmogorov time-scale, ν_u the unburned gas dynamic viscosity, $\sigma = 0.26\, ln\,(L_t/\eta)$ is the standard deviation of the assumed log-normal distribution of the turbulent dissipation rate ε, and $\varepsilon_{cr} = 15\nu_u g_{cr}^2$ is the turbulent dissipation rate at the critical rate of strain g_{cr}.

For laminar and steady conditions the critical rate of strain g_{cr} may be obtained numerically [40], but such strategies are not suitable for applications because different steady-state problems, associated for example to different geometries, produce broad changes of g_{cr}. Furthermore, in turbulent flows g_{cr} is much larger than in steady-state situations due to the short life-time of small eddies. In simulations it is reasonable to use algebraic expressions suggested by dimensional analysis, such as $g_{cr} \approx \tau_{ch}^{-1}$ [41].

Original Bray's Eqn. (2.28) could be here adapted in the framework of subgrid scale modelling and according to the present modelled premixed combustion regimes. However, the extinction trends predicted by Eqn. (2.28) do not agree at all with those found from both experiments and direct numerical simulations, that provide in fact similar trends [9, 33, 42].

The standard deviation of the turbulent dissipation rate distribution can also be written as

$$\sigma = 0.26\, ln\left(\frac{l_{\Delta}}{\eta}\right) = 0.195\, lnRe_{\Delta} = 0.195\, ln\left[Pr^{-1}\left(\frac{l_{\Delta}}{\delta_{\mathcal{F}}}\right)\left(\frac{u'_{\Delta}}{\mathcal{S}_{\mathcal{L}}}\right)\right]. \tag{2.29}$$

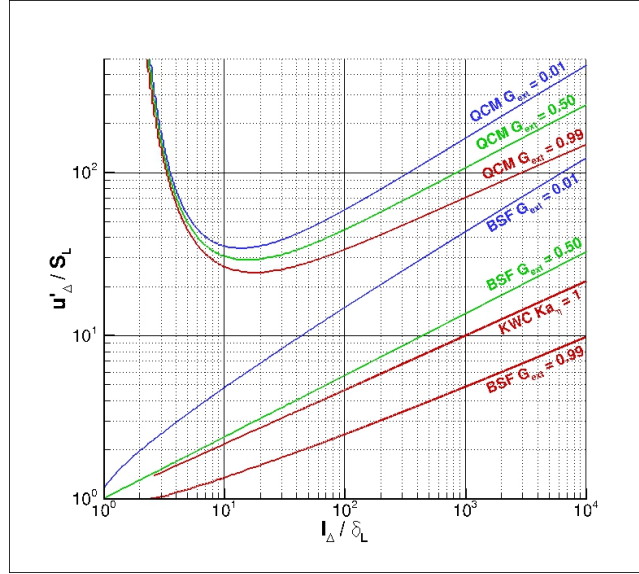The local Reynolds number Re_{Δ} has to be larger than one.

Figura 2.2: Comparison of the two quenching criteria analyzed. In particular, three $\mathcal{G}_{ext}$ isolines are shown on the plane of the standard combustion diagram for both Bray's stretch factor model (BSF) with $Pr = 1$ and the *quenching cascade model* (QCM). The $Ka_\eta = 1$ line related to the Klimov-Williams criterion (KWC) is also shown for comparison.

Assuming $\varepsilon_{cr} = 15 \, \nu_u g_{cr}^2 \approx 15 \, \nu_u \tau_{ch}^{-2}$ and $\varepsilon \approx 15 \, \nu_u \tau_{st}^{-2}$, τ_{st} being the characteristic stretching time, the ratio $\varepsilon_{cr}/\varepsilon$ can be written as

$$\frac{\varepsilon_{cr}}{\varepsilon} \approx \left(\frac{\tau_{st}}{\tau_{ch}} \right)^2 = Ka^{-2} \,, \tag{2.30}$$

$Ka = \tau_{ch}/\tau_{st}$ being the Karlovitz number. In a turbulent flow, the (longitudinal) Taylor microscale λ_g could be used to define the mean spatial velocity gradient u'_Δ/λ_g. With this assumption, $\tau_{st} = \lambda_g/u'_\Delta$, that is also equal to the Kolmogorov eddy turn-over time, $\tau_\eta = \eta/u'_\eta$, as shown in Eqn. (1.11), it follows:

$$\frac{\varepsilon_{cr}}{\varepsilon} \approx Ka_{\lambda_g}^{-2} \equiv Ka_\eta^{-2} = Da_\Delta^{I2} Re_\Delta^{-1} = Pr \left(\frac{l_\Delta}{\delta_\mathcal{F}} \right) \left(\frac{u'_\Delta}{\mathcal{S}_\mathcal{L}} \right)^{-3} \,, \tag{2.31}$$

It is observed that assuming $\tau_{st} = \tau_\eta$, the smallest eddies, i.e., the Kolmogorov dissipative scales, are assumed to be able to affect the flame front. Hence, a first criticism is that the dissipative scale η may in fact be too small to effectively stretch the flame front, as it was observed in Section 1.1. Furthermore, viscous dissipation at η scales cannot be neglected, causing their dissipation before they have a chance of quenching the flame. This theoretical basis coupled with the experimental observation of actual flames resisting to strain more than predicted by the Karlovitz criterion, lead Peters [6] to shift the Karlovitz criterion from $Ka_\eta = 1$ to $Ka_\eta = 100$ [21] [22, p. 78-79]. This is equivalent to say that the scale that can effectively stretch the flame front and cause extinction is larger than η. This is in agreement with the concept of the smallest eddy surviving scale l^*, suggested in this work, in modeling eddies / flame front interaction (see Section 2.1.1), according to which, scales smaller than l^* do not affect the flame front. However, even considering these effects do not alter the main trends of Bray's function.

The $\mathcal{G}_{ext}$ Bray's function resulting from Eqns. (2.28), (2.29) and (2.31) is plotted in the standard combustion diagram, i.e., versus $l_\Delta/\delta_\mathcal{F}$ and $u'_\Delta/\mathcal{S}_\mathcal{L}$ assuming $Pr = 1$. It is observed that quenching predictions related to this extinction function are quite similar to those provided by the Klimov-Williams criterion (see Section 1.1, Fig. 1.2) and do not agree with those related to the *quenching cascade model* [42] proposed in Section 2.6.2, closer to experiments and direct numerical simulation predictions.

2.6.2 The Quenching Cascade Model

A model that can be easily used to predict quenching is the so called *quenching cascade model* [42], that compares quite well with experimental and direct numerical simulation data on quenching [33, p. 212-214].

Here, only the algorithm of the quenching cascade model is reported redirecting the reader to the original article [42] for the theoretical part. The main assumptions at the base of the model are:

1. however strong the vortex strain may be, the time required to quench the flame is the same and it is given by $\tau_{ch} = \delta_{\mathcal{F}}/\mathcal{S}_{\mathcal{L}}$;

2. only eddies with large characteristic velocity u'_l (at least $\geq \mathcal{S}_{\mathcal{L}}$) are able to quench the flame;

3. if the eddy turnover-time τ_l is smaller than the chemical time τ_{ch}, such eddies cannot quench the flame, i.e., the eddies able to quench the flame have $Da_l^I \geq 1$;

4. a temporal sequence of approximately τ_{ch}/τ_l consecutive eddies of size l with large u'_l must exist to induce actual quenching;

5. the mean eddy time-scale τ_l is estimated considering a multifractal description of turbulence with intermittency;

6. a discrete set of scales is recursively generated.

With these assumptions, the *quenching cascade model* estimates the total fraction of flame surface undergoing quenching during a time τ_{ch} as

$$\mathcal{P}_q \left(\frac{l_\Delta}{\delta_{\mathcal{F}}}, \frac{u'_\Delta}{\mathcal{S}_{\mathcal{L}}} \right) = \frac{1}{2} \left\{ 1 + tanh \left[sgn[x] \, x^2 \right] \right\}, \tag{2.32}$$

where $tanh$ is the hyperbolic tangent function, sgn is the sign function, and

$$x \left(\frac{l_\Delta}{\delta_{\mathcal{F}}}, \frac{u'_\Delta}{\mathcal{S}_{\mathcal{L}}} \right) = \left[log_{10} \left(\frac{u'_\Delta}{\mathcal{S}_{\mathcal{L}}} \right) - g \left(\frac{l_\Delta}{\delta_{\mathcal{F}}} \right) \right] \sigma^{-1} \left(\frac{l_\Delta}{\delta_{\mathcal{F}}} \right), \tag{2.33}$$

with

$$g \left(\frac{l_\Delta}{\delta_{\mathcal{F}}} \right) = \left(0.7 + \frac{1}{s} \right) e^{-s} + \left(1 - e^{-s} \right) \left(1 + 0.36 \, s \right) \tag{2.34}$$

$$s \left(\frac{l_\Delta}{\delta_{\mathcal{F}}} \right) = log_{10} \left(\frac{l_\Delta}{\delta_{\mathcal{F}}} \right)$$

and

$$\sigma \left(\frac{l_\Delta}{\delta_{\mathcal{F}}} \right) = 0.04 \, log_{10} \left(\frac{l_\Delta}{\delta_{\mathcal{F}}} \right). \tag{2.35}$$

Finally, the extinction or stretch factor $\mathcal{G}_{ext} \leq 1$ in Eqn. (1.32) is in this work modeled as:

$$\mathcal{G}_{ext} = 1 - \mathcal{P}_q. \tag{2.36}$$

Three $\mathcal{G}_{ext}$ isolines of the *quenching cascade model* are shown in Fig. 2.2, where they are compared with the associated isolines of Bray's stretch factor and the Klimov-Williams criterion. In particular, the three red lines corresponding to $\mathcal{G}_{ext} = 0.99$ for the *quenching cascade model* and Bray's stretch factor and to $Ka_\eta = 1$ for the Klimov-Williams criterion, should be compared. Above these red lines extinction is predicted at different levels by these models. The extinction region predicted by the *quenching cascade model* has been validated with experimental data [9, 33, 42], hence, high velocity fluctuations are required to produce localized flame quenching.
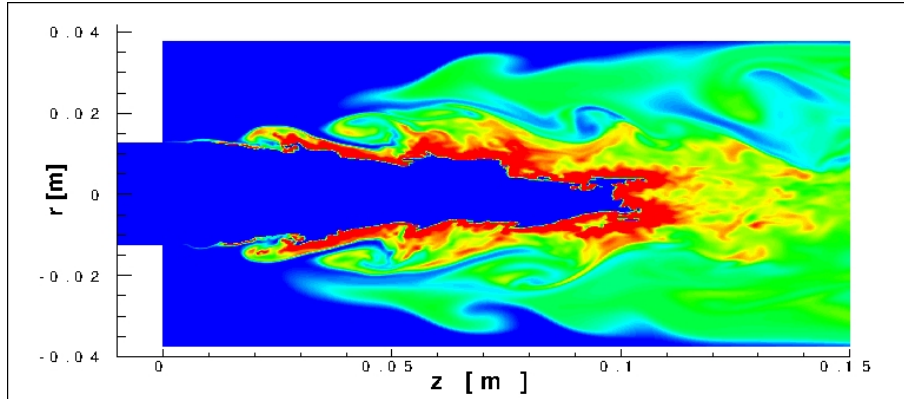
Figura 2.3: Instantaneous OH radical mass fraction distribution on a plane from the Large Eddy Simulation of the PSI test case.

2.7 Model Validation and Conclusions

It was initially planned to validate the new suggested model with a test case experimentally studied at PSI [43], consisting in a confined premixed turbulent syngas / air flame at 5 bar, a picture of which is reported in Fig. 2.3. This test case is close to gas turbine industrial applications (apart from swirling) and lets also to analyze the effects due to the presence of hydrogen. However, the available measurements are not sufficient for a complete validation of a new model.

Hence, it was decided to looking for other cases in literature. Two test cases were selected, here named as BELL and SANDIA. These cases have many numerical and experimental data to compare with. Both are slot burners that produce an unconfined Bunsen flame at 1 atm and consist of three adjacent rectangular burners: the central one injects a fresh mixture of methane and air, while the two side burners inject hot combustion products of the same central mixture. They are formally similar, but with different Reynolds numbers and then different turbulence levels. Apart from the available experimetal and numerical data to compare with, these test cases were chosen because a slot Bunsen flame represents one of the major categories of turbulent premixed combustion.

The BELL test case was experimentally investigated at the Department of Mechanical Engineering of the Purdue University(USA) [44], and numerically studied by means of Direct Numerical Simulation at the Center for Computational Science and Engineering of the Lawrence Berkeley National Laboratory [45]. The central burner and the two side burners are separated by two 2 mm sidewalls; each of the three burners has a cross-section of 2.5×5 cm^2 and a length of 20 cm and are fed with a stoichiometric mixture of methane and air. The central burner is used to create the Bunsen flame, while the side burners contain flat flames to produce hot products at the same velocity of the products of the Bunsen flame; this strategy avoids shear layers, and unwanted turbulence, that could be originated at the boundaries when the products meet the room air. The computational domain is $7.5 \times 5 \times 10$ cm^3 (x, y, z, z being the streamwise direction) and begins at the burner exit. Periodic conditions are applied along the minimum size (spanwise) direction, y. The reactant mixture with an equivalence ratio of $\Phi = 1$ is injected from the central slot with a bulk velocity of 3 m s^{-1} and at 298 K. The velocity of the coflow stream is 7 m s^{-1}. The central jet Reynolds number is 2678, based on the width of the jet, 2.5 cm, its bulk velocity, and the dynamic viscosity $2.8 \cdot 10^{-5}$ m^2 s^{-1}. The central jet turbulent Reynolds number is 56, based on the rms streamwise velocity fluctuation, 0.3 m s^{-1}, the integral scale, 5.2 mm, and the previous dynamic viscosity. Turbulence at the inlet of the central jet is generated in the experiment by means of a grid made of stainless steel wires that are 0.5 mm in diameter, and that have openings between the wires each of 2×2 mm^2. From experiments, the integral length scale is $L_t = 5.2$ mm and the Kolmogorov scale is $\eta = 0.2$ mm. The laminar flame speed and flame front thickness are $\mathcal{S}_{\mathcal{L}} = 0.38$ m s^{-1} and $\delta_{\mathcal{F}} = 0.35$ mm, respectively. Hence, $u'_{rms}/\mathcal{S}_{\mathcal{L}} = 0.71$ and $L_t/\delta_{\mathcal{F}} = 14.85$. Inlet turbulence in the simulation is artificially produced by means of a synthetic turbulence generator implemented from [46]. In particular, the spatial
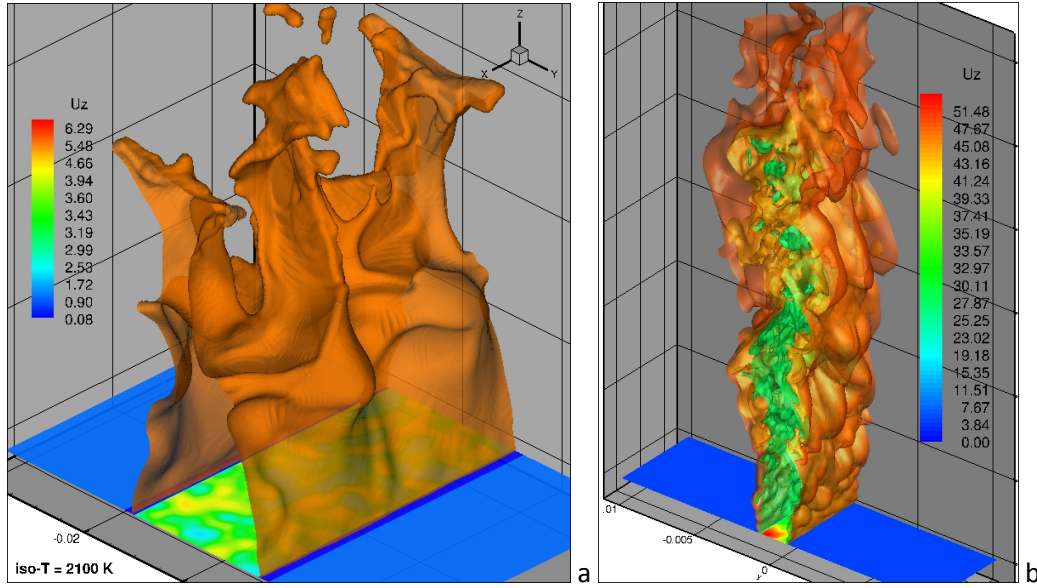
Figura 2.4: Instantaneous fields of the Large Eddy Simulations of the two slot burner test cases: (a) BELL, (b) SANDIA. The transversal inlet plane in both pictures shows the streamwise velocity, evidencing inlet turbulent fluctuations. The iso-surfaces are related to temperature: 1900 K in (a), 1100, 1900 and 2050 K in (b).

correlation length scales and velocity fluctuations provided as input to this generator are: $L_{zz} = 5.2\,\text{mm}$, $L_{xx} = L_{yy} = 2\,\text{mm}$, $u'_z = 0.3\,\text{m s}^{-1}$, $u'_x = u'_y = u'_z/1.3 = 0.263\,\text{m s}^{-1}$, having used typical correlations found in turbulent flows behind grids [47, p. 94-99].

The SANDIA test case was numerically defined and studied by means of Direct Numerical Simulation at Sandia National Laboratories [48, 49] and by means of Large Eddy Simulation at the Dept. of Mechanical Engineering of Stanford University [50]. The central slot has a cross-section of $1.8 \times 2.8\,\text{mm}^2$. The computational domain is $10 \times 2.8 \times 30\,\text{mm}^3$ (x, y, z, z being the streamwise direction). Periodic conditions are applied along the minimum size (spanwise) direction, y. Spatial transition from the central jet to the coflow along the x direction is obtained by means of a hyperbolic tangent function. The reactant mixture with an equivalence ratio of $\Phi = 0.7$ is injected from the central slot with a bulk velocity of $100\,\text{m s}^{-1}$ and at $800\,\text{K}$. The velocity of the coflow stream is $25\,\text{m s}^{-1}$. The central jet Reynolds number is 2100, based on the width of the jet, $1.8\,\text{mm}$, its bulk velocity, and the dynamic viscosity $8.57 \cdot 10^{-5}\,\text{m}^2\,\text{s}^{-1}$. The central jet turbulent Reynolds number is 252, based on the rms velocity fluctuation, $18\,\text{m s}^{-1}$, the integral scale, $1.2\,\text{mm}$, and the previous dynamic viscosity. Turbulence at the inlet of the central jet is forced to be homogeneous and isotropic. The integral length scale is $L_t = 1.2\,\text{mm}$, that is also the longitudinal spatial correlation length; the transverse spatial correlation lengths are half of the longitudinal one, due to the isotropy condition. The laminar flame speed and flame front thickness at these conditions are $\mathcal{S}_{\mathcal{L}} = 1.8\,\text{m s}^{-1}$ and $\delta_{\mathcal{F}} = 0.3\,\text{mm}$, respectively. Hence, $u'_{rms}/\mathcal{S}_{\mathcal{L}} = 10$ and $L_t/\delta_{\mathcal{F}} = 4$; $Ka_\eta = 225$, $Da_{L_t}^I = 0.4$, thus locating this flame into the broken reaction zones regime of the standard combustion diagram, where turbulence is expected to strongly influence premixed flame structures. Also in this simulation the homogeneous isotropic inlet turbulence is artificially produced by means of a synthetic turbulence generator implemented from [46]. In particular, the spatial correlation length scales and velocity fluctuations provided as input to this generator are: $L_{zz} = 1.2\,\text{mm}$, $L_{xx} = L_{yy} = L_{zz}/2 = 0.6\,\text{mm}$, $u'_z = u'_x = u'_y = 18\,\text{m s}^{-1}$ with no shear stresses (the Reynolds stress tensor is diagonal) [51].

Instantaneous distributions of the main quantities of the suggested model are shown in Figs. 2.5 and 2.6 for the BELL test case. Although the low local turbulence level, several combustion regimes are experienced in this flame, and also localized exinctions may take place, as evidenced by the $\mathcal{G}_{ext}$ function. Temperature distribution is used to mark the flame front region.

In order to validate the model presented in this work, different simulations with different spatial resolution
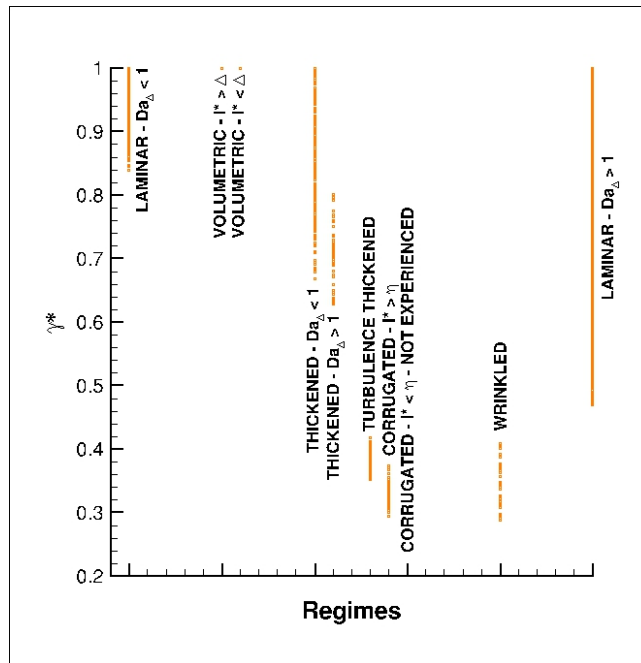
Figura 2.5: Instantaneous reacting volume fraction distribution along with the modelled subgrid combustion regimes. This distribution is associated to the flowfield of the BELL test case in Fig. 2.4a.

are required. Due to the more time needed to develop the theoretical part and to find new test cases, the validation is not yet concluded and will be run for some other few months. After this first validation phase, also the PSI test case will be considered to analyze the effects due to the presence of hydrogen.
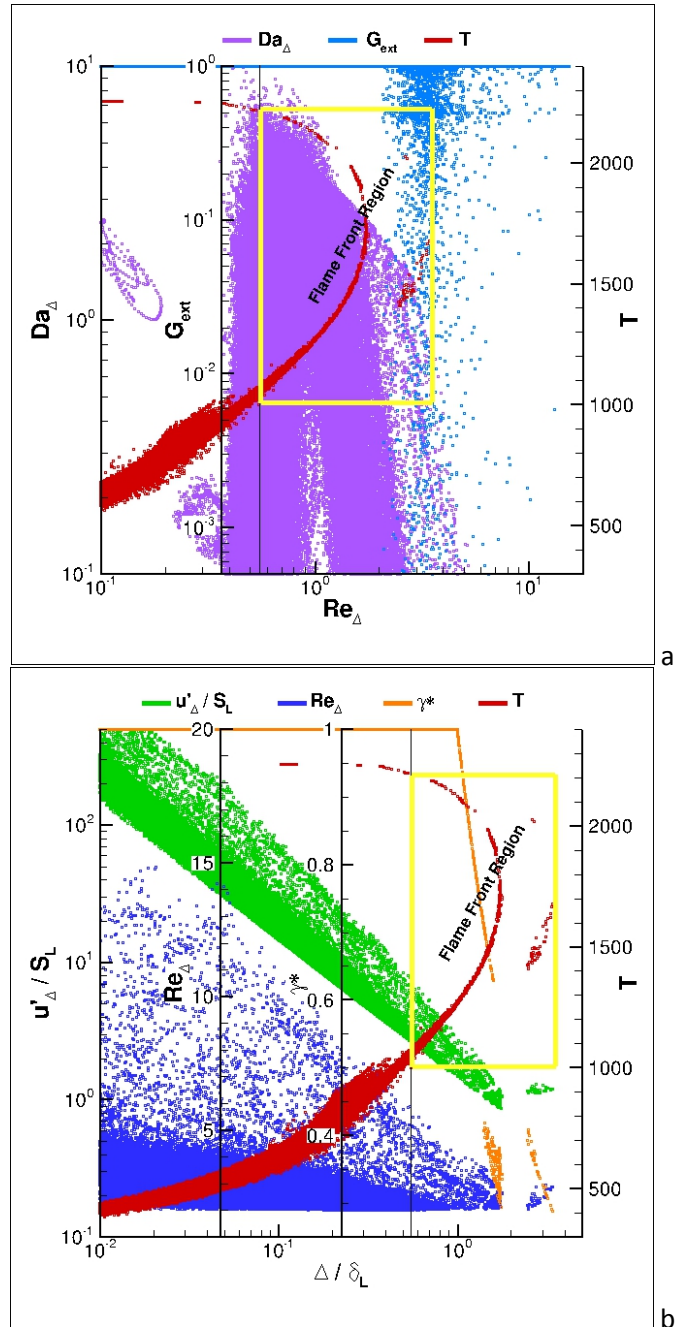
Figura 2.6: Instantaneous distributions associated to the flowfield of the BELL test case in Fig. 2.4a. In particular: (a) distribution of the local Da_Δ^I and $\mathcal{G}_{ext}$ function versus the local Re_Δ; (b) spectral diagram reporting also the distribution of Re_Δ and γ^*. Temperature distribution is also shown to mark the region related to the flame front.

Bibliografia

[1] Williams F.A. *Combustion Theory*. Addison-Wesley Publishing Company, 2nd edition, 1985.

[2] Barrere M. Modeles de combustion. *Revue Gen. Thermique*, 148:295, 1974.

[3] Bray K.N.C. Turbulent flows with premixed reactants in turbulent reacting flows. In Libby P.A. and Williams F.A., editors, *Topics in Applied Physics*, volume 44, page 115. Springer, 1980.

[4] Borghi R. On the structure and morphology of turbulent premixed flames. In Bruno C. and Casci C., editors, *Recent Advances in Aerospace Science*, page 117. Plenum, 1985.

[5] Borghi R. Turbulent combustion modelling. *Progress in Energy and Combustion Science*, 14:245--292, 1988.

[6] Peters N. Laminar flamelet concepts in turbulent combustion. In *Twenty First Symposium (International) on Combustion*, page 1231, Pittsburg, 1986. The Combustion Institute.

[7] Abdel-Gayed R.G. and Bradley D. Criteria for turbulent propagation limits of premixed flames. *Combustion and Flame*, 62:61, 1985.

[8] Abdel-Gayed R.G. and Bradley D. Combustion regimes and the straining of turbulent premixed flames. *Combustion and Flame*, 76:213, 1989.

[9] Poinsot T., Veynante D., and Candel S. Quenching processes and premixed turbulent combustion diagrams. *Journal of Fluid Mechanics*, 228:561--606, 1991.

[10] Chomiak J. *Combustion: A study in Theory, Fact and Application*. Abacus Press / Gordon and Breach Science Publishers, New York, 1990.

[11] Darabiha N., Candel S., and Marble F. The effect of strain rate on a premixed laminar flame. *Combustion and Flame*, 64:203, 1986.

[12] Giovangigli V. and Smooke M.D. Extinction of strained premixed laminar flames with complex chemistry. *Combustion Science and Technology*, 53:23, 1987.

[13] Ishizuka S. and Law C.K. An experimental study on extinction of stretched premixed flames. In *Nineteenth Symposium (International) on Combustion*, page 327, Pittsburg, 1982. The Combustion Institute.

[14] Sato J. Effects of lewis number on extinction behavior of premixed flames in a stagnation flow. In *Nineteenth Symposium (International) on Combustion*, page 1541, Pittsburg, 1982. The Combustion Institute.

[15] Law C.K., Zhu D.L., and Yu G. Propagation and extinction of stretched premixed flames. In *Twenty First Symposium (International) on Combustion*, page 1419, Pittsburg, 1986. The Combustion Institute.

[16] Candel S. and Poinsot T. Flame stretch and the balance equation for the flame area. *Combustion Science and Technology*, 70:1, 1990.

[17] Libby P., Linan A., and Williams F. Strained premixed laminar flames with non-unity lewis number. *Combustion Science and Technology*, 34:257, 1983.

[18] Karlovitz B. Turbulent flames. In *Fourth Symposium (International) on Combustion*, pages 613--620, Baltimore, 1953. The Combustion Institute.

[19] Glassman I. *Combustion*. Academic Press, San Diego, 3rd edition, 1996.

[20] Kolmogorov A.N. *Dokl. Akad. Nauk SSSR*, 30:299, 1941.

[21] Peters N. The turbulent burning velocity for large-scale and small-scale turbulence. *Journal of Fluid Mechanics*, 384:107--132, 1999.

[22] Peters N. *Turbulent Combustion*. Cambridge, 2000.

[23] Bird R.B., Stewart W.E., and Lightfoot E.N. *Transport Phenomena*. John Wiley and Sons, New York, 2nd edition, 2002.

[24] Kuo K.K. *Principles of Combustion*. John Wiley & Sons, New York, 1986.

[25] Domingo P., Vervisch L., Payet S., and Hauguel R. DNA of a premixed turbulent V flame and LES of a ducted flame using a FSD-PDF subgrid scale closure with FPI-tabulated chemistry. *Combustion and Flame*, 143:566--586, 2005.

[26] Gülder Ö.L., Smallwood G.J., Wong R., Snelling D.R., and Smith R. Flame front surface characteristics in turbulent premixed propane/air combustion. *Combustion and Flame*, 120:407--416, 2000.

[27] Giacomazzi E., Battaglia V., and Bruno C. The coupling of turbulence and chemistry in a premixed bluff-body flame as studied by LES. *Combustion and Flame*, 138(4):320--335, 2004.

[28] Giacomazzi E., Favini B., Bruno C., Picchia F.R., and Arcidiacono N. LES of H2/CH4/Air turbulent non-premixed flame. In *European Combustion Meeting*, 25-28 October 2003. Orleans, France.

[29] Giacomazzi E., Picchia F.R., Arcidiacono N., Cecere D., Donato F., and Favini B. Unsteady simulation of a CO/H2/N2/Air turbulent non-premixed flame. *Combustion Theory and Modeling*, 12(6):1125--1152, 2008.

[30] Giacomazzi E., Cecere D., Donato F., Picchia F.R., Arcidiacono N., Daniele S., and Jansohn P. LES analysis of a syngas turbulent premixed dump-combustor at 5 bar. In *XXXIII Event of the Italian Section of the Combustion Institute and II S4FE*, http://www.combustioninstitute.it, 17-20 June 2010. Ischia, Italy.

[31] Gulder O.L. and Smallwood G.J. Inner cutoff scale of flame surface wrinkling in turbulent premixed flames. *Combustion and Flame*, 103:107--114, 1995.

[32] Roberts W.L., Driscoll J.F., Drake M.C., and Goss L.P. Images of the quenching of a flame by a vortex: to quantify regimes of turbulent combustion. *Combustion and Flame*, 94:58--69, 1993.

[33] Poinsot T. and Veynante D. *Theoretical and Numerical Combustion*. Edwards, Philadelphia, 2nd edition, 2005.

[34] Zimont VL. The theory of turbulent combustion at high reynolds numbers. *Combustion Explosions and Shock Waves*, 15:305--311, 1979.

[35] Zimont VL.and and Lipatnikov A.N. A numerical model of premixed turbulent combustion of gases. *Chem. Phys. Reports*, 14(7):993--1025, 1995.

[36] Zimont VL.and Biagioli F. and Syed K. Modelling turbulent premixed combustion in the intermediate steady propagation regime. *Progress in Computational Fluid Dynamics*, 1(1-3):14--28, 2001.

[37] Lipatnikov A.N. and Chomiak J. Turbulent flame speed and thickness: Phenomenology, evaluation, and apllication in multi-dimensional simulations. *Progress in Energy and Combustion Science*, 28:1--74, 2002.

[38] Bray K.N.C. Methods of including realistic chemical reaction mechanisms in turbulent combustion models. In Jager W., editor, *Complex Chemical Reactions Systems. Mathematical Modelling and Simulation*, pages 356--375, Heidelberg, 1987. Springer.

[39] Sathiah P., van Haren S., Komen E., and Roekaerts D. The role of cfd combustion modeling in hydrogen safety management—ii: Validation based on homogeneous hydrogen–air experiments. *Nuclear Engineering and Design*, 252:289--302, 2012.

[40] Rogg B. Response and flamelet structure of stretched premixed methane/air flames. *Combustion and Flame*, 73:45--65, 1988.

[41] Zimont VL. and Biagioli F. Gradient, counter-gradient transport and their transition in turbulent premixed flames. *Combustion Theory and Modelling*, 6:79--101, 2002.

[42] Meneveau C. and Poinsot T. Stretching and quenching of flamelets in premixed turbulent combustion. *Combustion and Flame*, 86:311--332, 1991.

[43] Daniele S., Mantzaras J., Jansohn P., Denisov A., and Boulouchos K. Flame front/turbulence interaction for syngas fuels in the thin reaction zones regime: turbulent and stretched laminar flame speeds at elevated pressures and temperatures. *J. of Fluid Mechanics*, 724:36--68, 2013.

[44] Filatyev A., Driscoll J.F., Campbell D., and Carter D. Measured properties of turbulent premixed flames for model assessment, including burning velocities, stretch rates, and surface densities. *Combustion and Flame*, 141:1--21, 2005.

[45] Bell J.B., Day M.S., Grcar J.F., Lijewsky M.J., Driscoll J.F., and Filatyev S.A. Numerical simulation of a laboratory-scale turbulent slot flame. In *Proceedings of the 31th Symposium International on Combustion, The Combustion Institute*, volume 31, pages pp. 1299--1307, 2007.

[46] Klein M., Sadiki A., and Janicka J. A digital filter based generation of inflow data for spatially developing direct numerical or large eddy simulations. *J. of Computational Physics*, 186:652--665, 2003.

[47] Garde R.J. EDITOR =.

[48] Sankaran R., Hawkes E.R., Chen J.H., Lu T., and Law C.K. Structure of a spatially developing turbulent lean methane-air bunsen flame. In *Proceedings of the 31th Symposium International on Combustion, The Combustion Institute*, volume 31, pages pp. 1291--1298, 2007.

[49] Chen J.H., Choudhary A., De Supinski B., De Vries M., Hawkes E.R., Klasky S., Liao W.K., Ma K.L., Mellor-Crummey J., Podhorski N., Sankaran R., Shende S., and Yoo C.S. Les of a premixed jet flame dns using a strained flamelet model. *Comput. Sci. Disc.*, 2, 2009.

[50] Knudsen E., Hawkes E.R., and Pitsch H. Les of a premixed jet flame dns using a strained flamelet model. *Combustion and Flame*, in press, Available online 5 August 2013:?--?, 2013.

[51] Gence J.N. Homogeneous turbulence. *Annual Review in Fluid Mechanics*, 15:201--222, 1983.